Osteocalcin: Promoter or Inhibitor of Hydroxyapatite Growth?

Mahdi Tavakol, ¹ Juan Liu, ¹ Samuel E. Hoff, ¹ Cheng Zhu, ¹ Hendrik Heinz^{1,2*}

Department of Chemical and Biological Engineering, University of Colorado Boulder, 3415
8Colorado Ave, Boulder, CO 80301, USA

² Materials Science and Engineering Program, University of Colorado Boulder, 3415 Colorado Ave, Boulder, CO 80301, USA

* Corresponding author: hendrik.heinz@colorado.edu

Abstract

Osteocalcin is the most abundant non-collagenous bone protein, vital for skeletal stability and repair. However, the function in bone remineralization and inhibition of bone growth has remained unclear. In this contribution, we explain the dual role of osteocalcin in nucleation of new calcium phosphate during bone remodeling and in inhibition of hydroxyapatite crystal growth at the molecular scale. The mechanism was derived using pH-resolved all-atom models for the protein, phosphate species, and hydroxyapatite, along with molecular dynamics simulations, experimental and clinical observations. Osteocalcin binds to (hkl) hydroxyapatite surfaces through multiple residues, identified in this work, and the fingerprint of binding residues varies as a function of (hkl) crystal facet and pH value. On balance, the affinity of osteocalcin to hydroxyapatite slows down crystal growth. The unique tri-calcium gamma-carboxylglutamic acid (Gla) domain hereby rarely adsorbs to hydroxyapatite surfaces and faces instead towards the solution. The Gla domain enables prenucleation of calcium phosphate for new bone formation at a slightly acidic pH value of 5. The growth of prenucleation clusters of calcium phosphate continues upon increase in pH value from 5 to 7, and is much less favorable, or not observed, on the native osteocalcin structure at and above neutral pH values of 7. The results provide mechanistic insight into the early stages of bone remodeling from the molecular scale, help inform mutations of osteocalcin to modify binding to apatites, and guide towards potential cures for osteoporosis, hyperosteogeny, and drug design.

Keywords: bone remodeling; osteocalcin; molecular dynamics; hydroxyapatite; phosphate mineralization; prenucleation clusters; gamma-carboxylglutamic acid; protein structure; protein-surface binding; acid-base equilibria

Introduction

Osteocalcin is among the ten most abundant proteins in the human body and the most common non-collagenous protein in bone. Deciphering the interaction of osteocalcin with hydroxyapatite crystals and the role of individual amino acids is critical to engineer biomineralization and work towards potential cures for osteoporosis and other skeletal diseases. The presence of osteocalcin in ectopic calcification sites has suggested a role in bone biomineralization that involves the generation and remodeling of hydroxyapatite (HAp). Several studies have characterized osteocalcin as a promoter for bone remodeling and, at the same time, also reported the inhibition of bone growth by osteocalcin. The different roles of osteocalcin are not well understood and the underlying molecular interactions with HAp surfaces and precursors of calcium phosphate in solution remain unknown, preventing progress towards molecular engineering and potential cures for skeletal diseases. For instance, engineering osteocalcin for bone remodeling could be utilized in treatments for osteoporosis. Conditions under which osteocalcin delays bone growth could be modified to support treatments for Paget's disease, and knowledge of the molecular mechanisms for mineralization can inform drug design.

Many clinical and experimental studies agree that osteocalcin supports the growth of new bone. For example, osteocalcin is present from the beginning of bone mineralization and growth in chicks. Decarboxylation of osteocalcin can lead to osteopenia which is characterized by a decrease in bone resorption and more pronounced decrease in bone formation, suggesting a significant role of osteocalcin and the Gla domain in bone remodeling. There is also a direct link associating higher amounts of osteocalcin in various bone types with decreased remodeling time. The furthermore, tooth enamel contains no osteocalcin and does not remodel while cortical bone contains more osteocalcin than the trabecular bone and the remodeling period is shorter.

At the same time, osteocalcin has also been shown to slow down bone growth. Bone growth was found to be higher in osteocalcin-deficient mice.⁴ Osteocalcin also decreased the rate of HAp crystal growth in laboratory studies⁶ and inhibited the crystallization of HAp at pH 7.4.⁵ The presence of chicken osteocalcin had a similar inhibitory effect on the seeded growth of HAp at pH 7.4.⁷ Adding osteocalcin to a solution of K₂HPO₄, CaCl₂ and KCl shows hindrance of mineralization,⁸ and HAp crystal growth in agarose-gel was delayed by osteocalcin.⁹

Overall, the data suggest that osteocalcin accelerates bone remodeling and delays bone growth. However, there is currently no mechanistic proposal for how osteocalcin achieves these functions and little understanding of the underlying biochemical processes, which makes the development of osteocalcin therapeutics for osteoporosis and hyperosteogeny challenging. Bone remodeling is known to occur in cavities formed on top of bones called bone remodeling compartments. ¹⁶⁻²⁰ Initially, osteoclasts resorb (dissolve) bone by decreasing the pH value below 5. ²¹⁻²³ Then, osteoblasts increase the pH value by exchange of H⁺ ions with Na⁺ ions, ²⁴ and the formation of new bone occurs. ²⁰ The borders of the bone remodeling compartment stain positive for osteocalcin, which hints at the significance of osteocalcin in bone remodeling. To-date, in-vitro studies have been carried out in solution conditions at pH values of 7 while we have not come across reports under critical in-vivo conditions of pH 5 during bone remodeling.

In this study, we capitalize on the recent availability of accurate molecular models and capabilities of molecular simulations, which are capable to help close these gaps.²⁵⁻²⁷ We interrogated the function of osteocalcin at the molecular scale and likely mechanisms of the onset of bone repair and regulation of bone mineralization. We utilized all-atom models of apatite minerals, phosphate species, and osteocalcin along with molecular dynamics simulations and free energy analysis, including realistic electrolyte conditions and the role of changing pH values

(Figure 1).²⁵⁻²⁷ We utilize the IFF-CHARMM36 force field, whereby hydroxyapatite, calcium phosphates, and aqueous solution (TIP3P water model) are represented by the INTERFACE force field (IFF)²⁵ and osteocalcin by the CHARMM36 force field.²⁸ IFF exceeds the reliability of density functional methods at much lower computational cost and provides access to a larger scale and has previously undergone rigorous validation. IFF captures the variable surface chemistry of hydroxyapatite,²⁷ the protonation state of calcium phosphates in agreement with pK values and IR data,²⁹⁻³¹ water interfacial energies in agreement with experimental measurements,²⁷ as well as specific binding of amino acids and proteins such as collagen in about one order of magnitude higher accuracy than alternative models or earlier techniques.^{29, 32, 33} The IFF models for apatites and phosphate species are also available as a community resource in the CHARMM-GUI Nanomaterials Modeler.³⁴ The CHARMM36 force field has been thoroughly validated for proteins, is a reliable choice for osteocalcin, and compatible with IFF and TIP3P water models.²⁸

The precise representation of pH-dependent surface chemistry of HAp,^{27, 32} calcium phosphates, and of osteocalcin in the models enables the study of dynamic molecular processes related to bone remodeling from pH values of 5 to 7. The pH dependent protonation states of hydroxyapatite surfaces have been extensively discussed previously^{29, 31} and involve mainly monohydrogen phosphate termination at pH 10, mainly dihydrogen phosphate termination at pH 5, and gradual dissolution at lower pH values (Figure 2). Attention to the pH conditions is essential to quantify biomolecular recognition, nucleation of calcium phosphate precursors,^{29, 31} and to understand biomolecular interfaces with on oxides, metals, and 2D nanostructures in prior experimental and simulation studies.³⁵⁻³⁹ Our study reveals first insight into osteocalcin function at the molecular scale and overcomes barriers of current experimental techniques in time-resolved tracking of molecular processes.

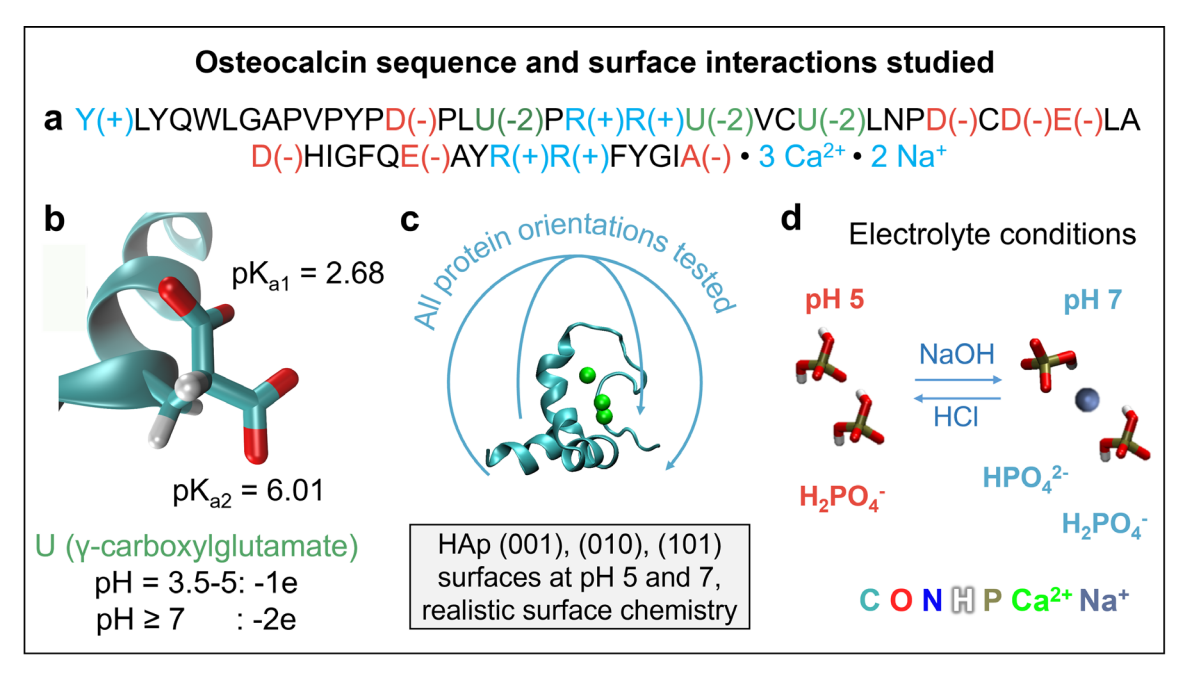


Figure 1. The composition of osteocalcin and role in bone mineralization. (a) Amino acid sequence and stoichiometry of porcine osteocalcin at pH 7 (positively charged residues = blue, negatively charged residues = red, electrically neutral residues = black). Three γ-carboxylglutamate residues (U) contain three bound calcium ions. (b) Structure and pK values of γ-carboxylglutamic acid (Gla). The side chain has a negative charge of -1e at pH 5 which changes to -2e at pH 7. The protonation state is critical for the formation and stability of calcium hydrogen phosphate prenucleation clusters. (c, d) Schematic of different protein orientations and changes in electrolyte conditions tested to elucidate binding to hydroxyapatite (hkl) surfaces at pH 5 and pH 7 via molecular dynamics simulation.

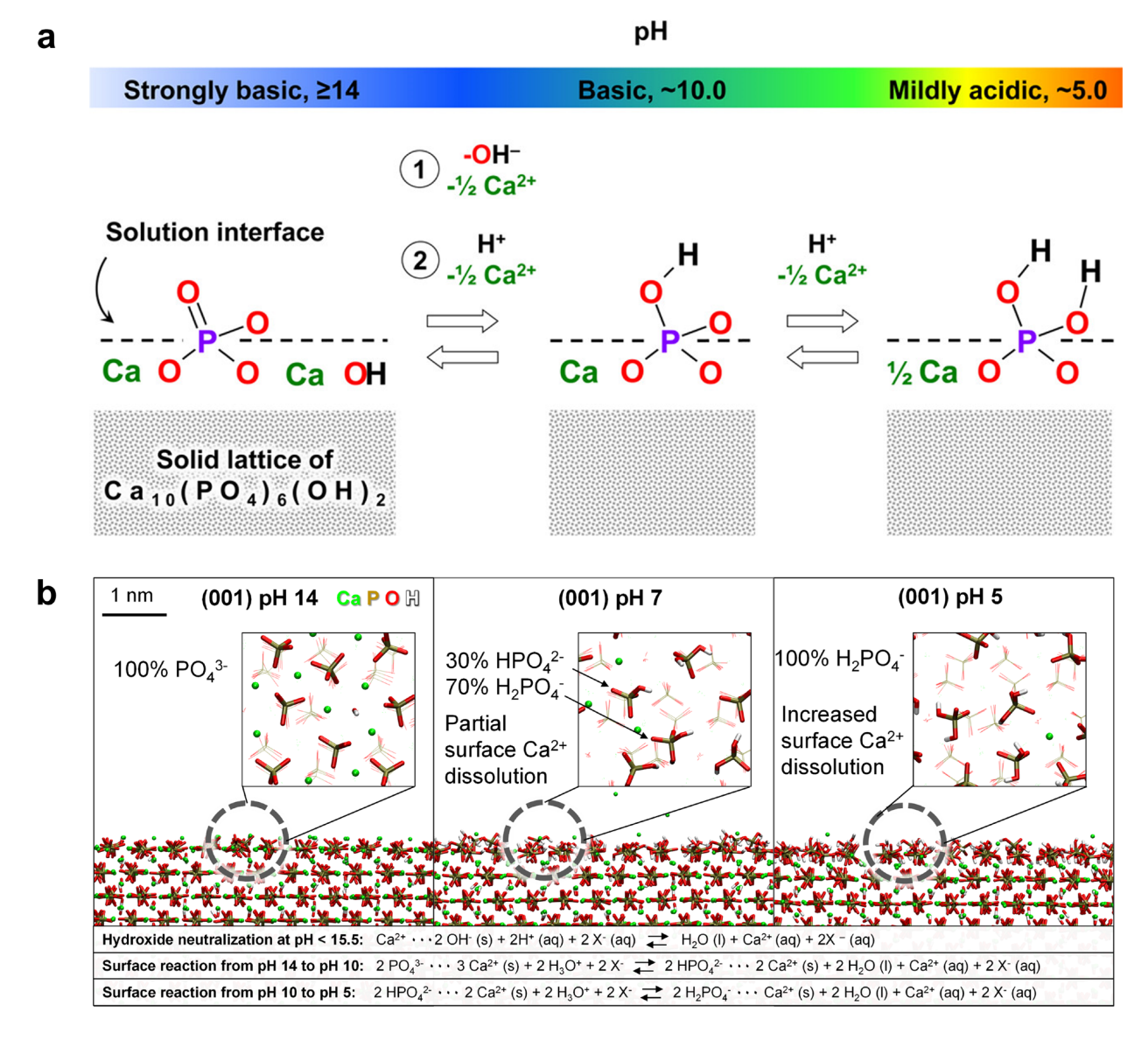


Figure 2. Important details of the HAp surface chemistry and representation in molecular models. HAP has the bulk formula Ca₁₀(PO₄)₆(OH)₂, however, HAp surface molecular layers exposed to electrolytes under physiological pH values have a very different composition that follow the pK values of water, phosphoric acid, supported by prior experimental characterization (see ref. ²⁷). (a) Interactions with water at pH values lower than 14 cause protonation and leaching of superficial hydroxide ions along with a stoichiometric amount of calcium ions. Increasing protonation of superficial phosphate ions leads to the formation of hydrogen phosphate and removal of a

stoichiometric amount of calcium ions. At pH values lower than 10, further protonation of hydrogen phosphate to dihydrogen phosphate and removal of further calcium ions occurs. Surface models for a specific pH value can be customized by corresponding stoichiometric changes to pristine hydroxyapatite surfaces and associated redistribution of atomic charges to maintain overall charge neutrality. (Reproduced with permission from ref. ²⁷). (b) As an example, we show side and top view of the (001) HAp surfaces at different pH values. (Left) At a pH = 14, neutralization of hydroxide ions (pK ~15.7) occurs and reduces the Ca²⁺ density relative to the cleavage planes in vacuum. The side view at pH = 14 with an inset of the top view shows 100% of phosphate ions (PO₄³⁻) on the surface and a high area density of calcium ions. (Middle) Continued protonation to pH = 7 leads to a mixture of 30% HPO₄²⁻ ions and 70% H₂PO₄⁻ ions on the surface, resulting in less than half the surface charge per area compared to pH 14. (Right) At pH = 5, the surface consists mostly of H₂PO₄ ions, with 30% less calcium ions present per surface area than at a pH value of 7. (Bottom) A summary of the acid-base reactions on the surface, consistent with pK values of phosphoric acid of 2.12, 7.21 and 12.44. The protonation/deprotonation reactions occur similarly on other (hkl) surfaces such as (010)/(020) (see ref. ²⁷). (Reproduced with permission from ref. ³²).

Results and Discussion

Osteocalcin is composed of 49 amino acids (Figure 1a). The uncommon amino acid γ -carboxylglutamate (abbreviation: U or Gla) (Figure 1b) forms a unique motif containing three calcium ions on the protein surface (Figure 1c). Large-scale molecular dynamics simulations and steered molecular dynamics calculations were utilized to reveal the interaction of osteocalcin with common (hkl) hydroxyapatite surfaces (Figure 1c, d) and calcium phosphate nucleation behavior across the protein surface at pH values of 5 and 7, which is critically influenced by the Gla domain.

The proposed role of osteocalcin in bone mineralization is as follows. (1) At pH 5, osteocalcin binds significantly to hydroxyapatite and inhibits crystal growth. Hereby, the tricalcium motif avoids contact with the hydroxyapatite surface. Surface phosphate species (dihydrogenphosphate) can dissolve, or are otherwise present in solution, and attracted to the tricalcium motif of osteocalcin. (2) An increase in pH value from 5 to 7 reduces osteocalcin binding to the mineral surface although crystal growth continues to be delayed by osteocalcin. Existing prenucleation clusters of calcium phosphate on the tricalcium motif grow larger. At pH 7, phosphate species are no longer attracted to bare tri-calcium sites and new mineralization no longer occurs.

Osteocalcin-Hydroxyapatite Interaction in Solution. Hydroxyapatite crystals are typically bounded by (001), (010), and (101) surfaces.²⁷ Partial dissolution of protonated phosphate species on these surfaces, such as Ca²⁺, H₂PO₄⁻, and HPO₄²⁻ ions, was observed as a result of the reaction of bulk hydroxyapatite with the biological buffer solution (Figure 2b and Figure 3). The partial solubility of the calcium phosphate species on the surfaces is consistent with experimental data. Osteocalcin shows favorable adsorption to the three common crystal surfaces at a pH value of 5 (Figure 3a-f). At this pH value, the mineral surface is mostly terminated by dihydrogenphosphate ions.^{32, 33} A higher pH value of 7 changes the surface chemistry to a mixture of dihydrogenphosphate ions and monohydrogenphosphate ions with a higher Ca-to-P ratio.^{30, 40} These differences induce desorption of osteocalcin from the (001) surface at pH 7 (Figure 3g, h) while the protein remains bound on the (010) surface (Figure 3i, j).Adsorption is also weaker on the (101) surface at pH 7 (Figure 3k, l) in comparison to pH 5. Therefore, the overall attraction of osteocalcin is high on the prismatic (010) surfaces at both pH values, somewhat reduced on (101) surfaces at pH 7, and largely eliminated on (001) surfaces at pH 7. Sustained binding at pH 7 to some crystal facets is consistent with the experimentally observed slowdown of crystal growth in the presence of osteocalcin.

At both pH values, the tri-calcium motif is not involved in binding to HAp and remains accessible to the solution phase (highlights in Figures 3 and Figure S1 in the Supporting Information). Only intermittent interactions with the hydroxyapatite (hkl) surfaces were observed (Figures 3 and 4). While we cannot completely rule out binding of the Gla domain to HAp (hkl) surfaces, we extensively sampled various binding conformations using different initial orientations and observed no significant binding. For example, starting with "perpendicular" orientations in which the tricalcium motif faces toward the surface lead to unbinding of the tricalcium motif from the surface during the simulation (Figure 3b, d, f, h, j, l). Snapshots with additional orientations are shown in Figure S1 in the Supporting Information.

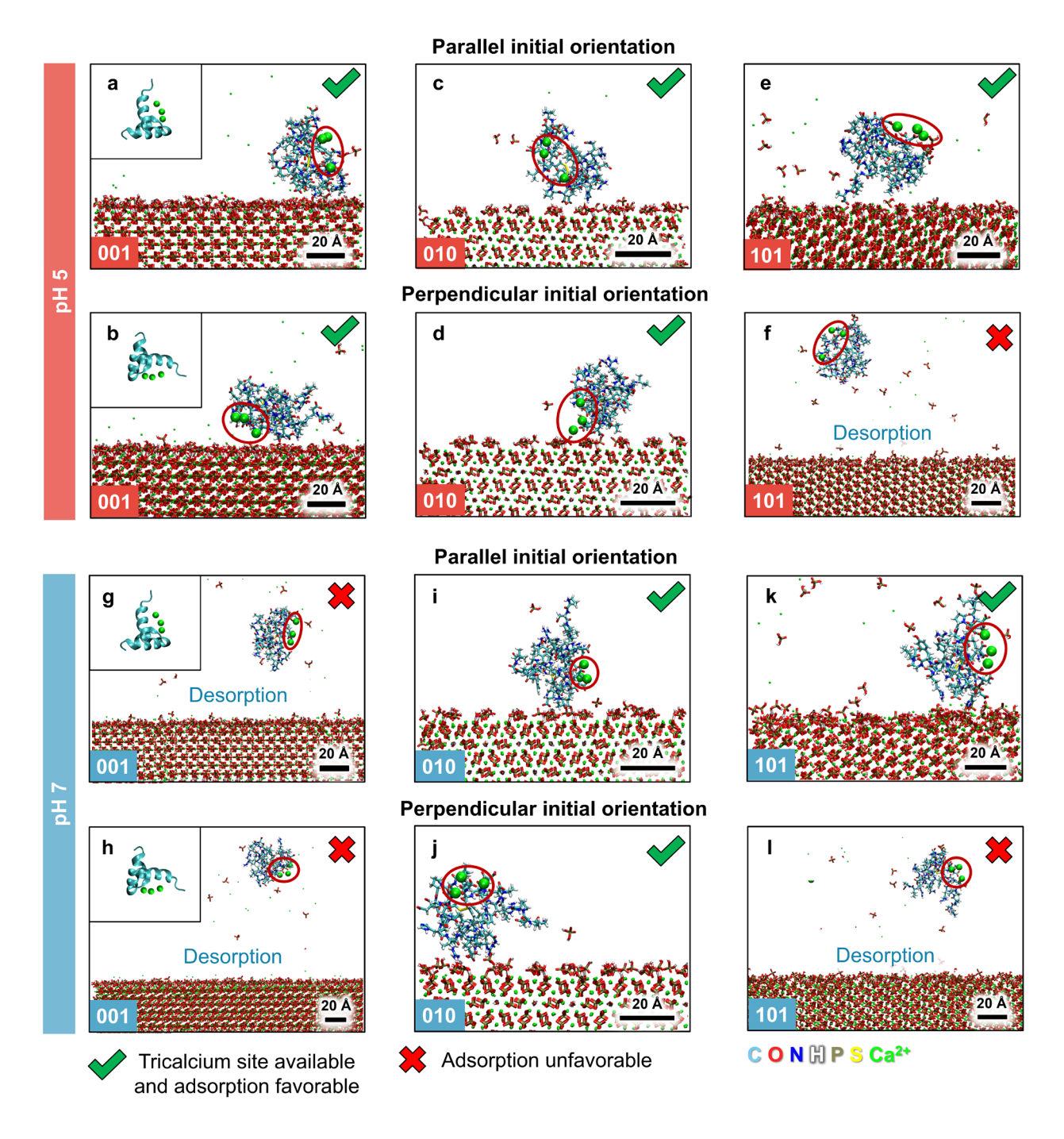


Figure 3. Interaction of osteocalcin with common hydroxyapatite (hkl) surfaces at pH values of 5 and 7. The protein is strongly attracted at pH 5, less attracted or desorbed at pH 7, and the tricalcium motif typically avoids contact with the surfaces (red circles). (a-f) Representative equilibrium configurations on the (001), (010), and (101) surfaces at pH 5 starting with parallel (inset in a) and perpendicular initial orientation (inset in b). The tricalcium motif assumes random

orientations and remains accessible from the solution (highlighted by red circles). (g-l) Representative equilibrium configurations on the (001), (010), and (101) surfaces at pH 7 starting with parallel and perpendicular initial orientation (see insets in g and h). Protein attraction is weaker on some surfaces and the tricalcium motif continues to avoid surface contact (highlighted by red circles). Snapshots are shown after more than 50 ns simulation time.

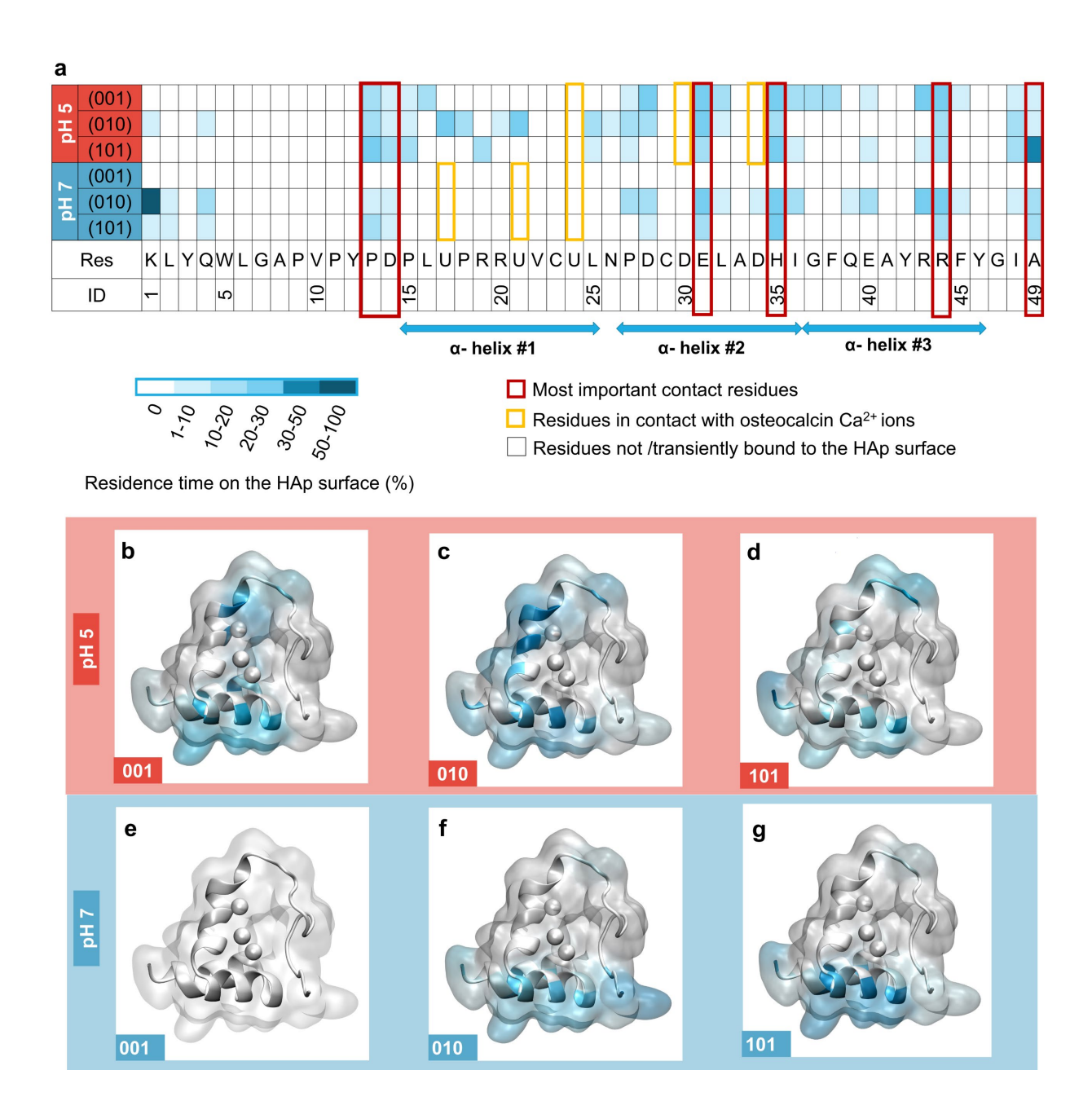


Figure 4. Contact residues for the adsorption of osteocalcin on different HAp facets at different pH values (boxes with blue shade). (a) Chart of residence times, equal to binding contribution, for each amino acid in osteocalcin as a function of hydroxyapatite crystal facet and pH value (a darker shade of blue depicts longer residence time). The most important binding residues are highlighted in dark red color. Residues in the Gla domain that attract calcium ions to the protein surface are marked in dark yellow and have only transient surface contact with HAp. The three helical regions

of osteocalcin are indicated using double sided blue arrows, and the remainder of the protein has random coil structure. (b-g) 3D representations of osteocalcin with the same color code as in (a) show the spatial distribution of binding and nonbinding residues to HAp at pH values of 5 (b-d) and 7 (e-g), including specific differences for the major crystal facets, i.e., the basal plane (001), the prismatic plane (010), and the (101) plane. Arg-44, Glu-31, His-35, and C-terminus-49 are the overall most important contact residues for the adsorption of osteocalcin to HAp. The data are based on 48 independent simulations for a total of 2.88 μs, including multiple replicas for each type of (hkl) surface and pH value.

Specific contributions to binding and the dynamics of the Gla domain were analyzed in more detail. The secondary structure of osteocalcin involves three α-helices (residues 15-25, 27-36, 37-46) and short random coils (Figure 4). Binding to HAp is mediated mainly by ion pairing via positively and negatively charged residues on the protein, as well as by additional hydrogen bonds. The observed binding patterns are sensitive to differences among (hkl) facets and solution pH values. At pH 5, the residues P13, D14, D28, E31, H35, R44 and A49 were found to be in contact with the HAp surface. Some changes in binding occur at pH 7, then including the residues Y1, P13, D14, P27, E31, H35, R44, and A49 (Figure 4 and Section S1 in the Supporting Information). The N-terminus (Y1) and the C-terminus (A49) bind at both pH values due to the charge (Figure 1a and Figure 4). Also, arginine (R44) binds through the positively charged guanidinium side group to negatively charged hydrogen phosphate groups on the HAp surface, aided by the conformational flexibility of the R side chains and the ability to form additional hydrogen bonds with hydrogen phosphate ions. Binding of histidine (H35) involves similar interactions, especially in the protonated state at pH 5. Glutamate (E31) binds via negatively charged carboxylate groups

to calcium ions on the HAp surface, whereby longer side chains than in aspartate (D28) enable more flexible, stronger binding.

At pH 5, binding of the tricalcium motif to the surface is unfavorable as the neighboring residues only partially compensate for the Ca²⁺ charge (Figure 1b). The resulting net positive charge of the Gla domain leads to moderate repulsion of the tri-calcium domain from the Ca²⁺-rich HAp surface, and this positive charge is critical to trigger phosphate mineralization as discussed below. At pH 5, the tricalcium motif assumes a modified structure with Ca²⁺ ions near U24, D30, and D34 (Figure 5a) that differs from the native structure at pH 7 with Ca²⁺ ions near U17, U21, and U24 (Figure 5a and Figure 4). Adsorption of osteocalcin to HAp at pH 5 is then stronger via the residues near P13 (Figure 3a, c, e) as well as D14 (Figure 3b, d and Figure 4) for α-helix #1, supported by longer and more flexible side chains.

At pH 7, the electrical charge of the three calcium ions bound to the protein is fully screened by six COO groups of the three Gla residues (Figure 1b), leading to lack of electrostatic interactions and similarly unfavorable binding to the HAp surface.

Earlier hypotheses of osteocalcin adsorption onto hydroxyapatite surfaces that assume binding via the tri-calcium motif have been made without knowledge of the details of the HAp surface chemistry and the structure of specific (hkl) facets,^{3, 8, 41, 42} and are incorrect according to the simulations. In these hypotheses, a specific binding affinity of the Gla domain to hydroxyapatite was reasoned by a similarity of calcium-calcium distances on the tricalcium site to those on freshly cleaved (010) surfaces of hydroxyapatite, which have values of 4 Å, 3.8 Å, and 7.1 Å on osteocalcin and presumably on hydroxyapatite.³ The structure of HAp surfaces in aqueous solutions at pH 5 and 7 is, however, entirely different from cleavage planes in vacuum (Figure 2).^{27, 32, 33} Under physiological conditions, the surface consists of disordered protonated phosphate

species with much lower Ca/P ratios than in the bulk mineral, supported by pK values of the acid-base equilibria, spectroscopy, hydration energies, and confirmation by molecular simulations.^{27, 30, 40} Dynamic dissociation-precipitation equilibria at the surface lead to a wide range of calcium-calcium distances on hydroxyapatite, which can be captured by MD simulations, and on balance turn the tricalcium motif away from the common hydroxyapatite surfaces (Figures 3 and 4)

Molecular Origin of Bone Remodeling. The protonation state and dynamics of the Gla domain are critical to understand nucleation and growth of new apatite (Figure 5a). At pH 5, osteocalcin is bound to the hydroxyapatite surface and some calcium dihydrogen phosphate units reversibly desorb from and adsorb onto the HAp surface, sustaining a certain solution concentration (Figure 3a-f). After several nanoseconds in solution, some dihydrogen phosphate ions migrate onto the tri-calcium site of osteocalcin and remain bound (Figures 5b, Figure 6a). To quantify these observations, we obtained free energy profiles of desorption of dihydrogen phosphate ions from the HAp (001) and (010) surfaces, as well as from the tri-calcium motif on the osteocalcin surface using steered molecular dynamics simulations (Figure 6b). The free energy of binding of dihydrogen phosphate ions to the tri-calcium motif of -4.0 kcal/mol is stronger than the free energies of binding to HAp (001) and (010) surfaces of -3.5 and -3.0 kcal/mol. Therefore, phosphate species from the mineral surface and elsewhere in solution prefer binding to the tri-calcium domain of osteocalcin over contributing to HAp crystal growth at pH 5.

The superficial dissolution of phosphate species from HAp and the formation of new prenucleation clusters on the osteocalcin surface can be regarded as the molecular origin of bone remodeling. According to prior experiments, bone remodeling begins near pH 5 after bone resorption at pH 4.5.²¹⁻²³ Laboratory experiments suggest that (1) resorption occurs at pH 4.5 or 5, (2) remodeling occurs after resorption, and (3) the pH increases from 5 to 7 during the remodeling

process while osteoblasts carry out bone mineralization at a pH of ~7.4 by releasing phosphate ions. 21-24 Our simulations show that a decreased pH value of pH 5 first induces a change in the arrangement of calcium ions on osteocalcin, and residues U17 and U21 no longer bind calcium ions (Figure 5a). On time average, one calcium ion migrates to D30 and to D34, which fully compensates the local electrical charge. Another calcium ions migrates to U24, and U24 then coordinates two calcium ions, consistent with a stabilizing effect of positively charged ions near the carboxyl end of an α -helix (Figure 4).⁴³ The effective charge of the U24 residue reaches up to +3e and negatively charged H₂PO₄⁻ ions adsorb onto this modified tricalcium site with two Ca²⁺ ions, as well as onto other partially protonated Gla residues containing one Ca²⁺ ion. The mobility of H₂PO₄ ions is thereby higher on sites with one calcium ion in comparison to U24 with two calcium ions (Figure 5b). The subsequent increase in pH value from 5 to 7 during bone remodeling changes the protonation state of Gla from -1 to -2 (Figure 5c) and of some dihydrogen phosphate ions (H₂PO₄¹⁻) to monohydrogen phosphate ions (HPO₄²⁻) (Figure 1d), leading to the attraction of more calcium ions to Gla and to the hydrogen phosphate species. Clusters of two protonated phosphate ions and four calcium ions were then observed (Figures 5c and Figure 6c). Further free energy calculations support that the monohydrogen phosphate ions are more strongly attracted to the prenucleated tricalcium site than dihydrogen phosphate ions because of stronger electrostatic attraction (Figure 6d). In support, calcium monohydrogen phosphate is also known to be the main precursor for HAp formation in experiments.⁴⁴ The increase in negative charge at the Gla site containing prenucleation clusters, combined with lower solubility of monohydrogen phosphate ions compared to dihydrogen phosphate ions continues to drive nucleation and growth of the cluster of adsorbed calcium ions and protonated phosphate ions on the osteocalcin surface. The computed adsorption free energies show that continued nucleation at higher pH value was more

favorable since each deprotonated oxygen atom of the protein-bound phosphate species coordinates with a calcium ion (Figure 5c). The structural definition of the Gla domain of the protein increases as the pH value changes from 5 to 7, shown by stable Ca-Ca distances over tens of nanoseconds (Figure S2a in the Supporting Information) and a decrease in root mean squared displacement of calcium ions and adsorbed H₂PO₄⁻ ions (Figure S2b in the Supporting Information). Hereby, the modified structure of osteocalcin at pH 5 does not recover to the native structure of osteocalcin at pH 7 after remodeling, on the time scale of the simulation, and structural differences appear to be related to the additional phosphate species adsorbed on the protein surface.

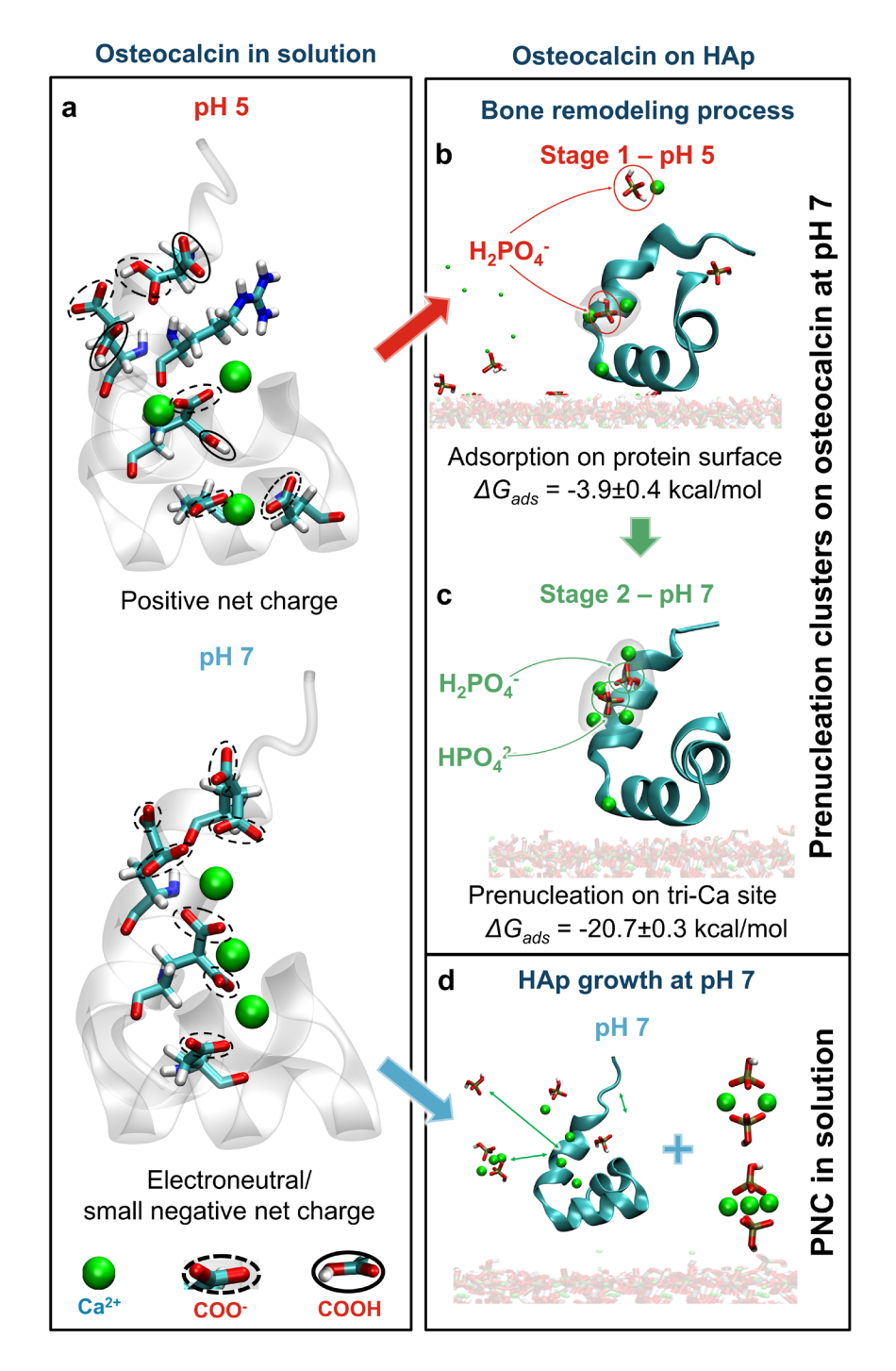


Figure 5. Role of osteocalcin in bone remodeling. (a) Osteocalcin assumes a modified structure at pH 5 compared to the native state at pH 7. Calcium ions on the tricalcium motif are more loosely bound and form a new pattern due to partial protonation of carboxylic acid groups in the U side chains (see highlights). Calcium ions are more tightly bound in the native state at pH 7 due to full

deprotonation of carboxylic acid side groups (see highlights). (b, c) Pathway of bone remodeling at the molecular scale. (b) As a first stage, at pH 5, osteocalcin binds to hydroxyapatite surfaces and dihydrogen phosphate ions partially dissolve from the surfaces into solution, illustrated for the (001) surface. Dihydrogen phosphate ions available in solution adsorb preferentially onto the osteocalcin surface rather than onto the hydroxyapatite surface (see text). Protein-bound calcium ions and adsorbed dihydrogen phosphate ions are represented as solid spheres. (c) As a second stage, the pH values increases to 7 and results in stronger adsorption of further protonated phosphate ions onto the initially adsorbed calcium phosphate cluster and onto the tricalcium motif of osteocalcin (now a mixture of HPO₄²⁻ and H₂PO₄⁻ ions). Calcium and phosphate ions are represented by solid spheres. (d) Changes in protein function at pH 7, starting with the native protein structure shown in lower part of the panel (a). Calcium and phosphate species do not adsorb onto the native protein surface at pH 7 and instead form stable prenucleation clusters in solution, such as tricalcium and dicalcium monohydrogen phosphate. Therefore, bare osteocalcin does not promote nucleation of new calcium phosphate, requiring protonation and a structural transition at lower pH values to initiate bone remodeling. Calcium ions are represented as green spheres.

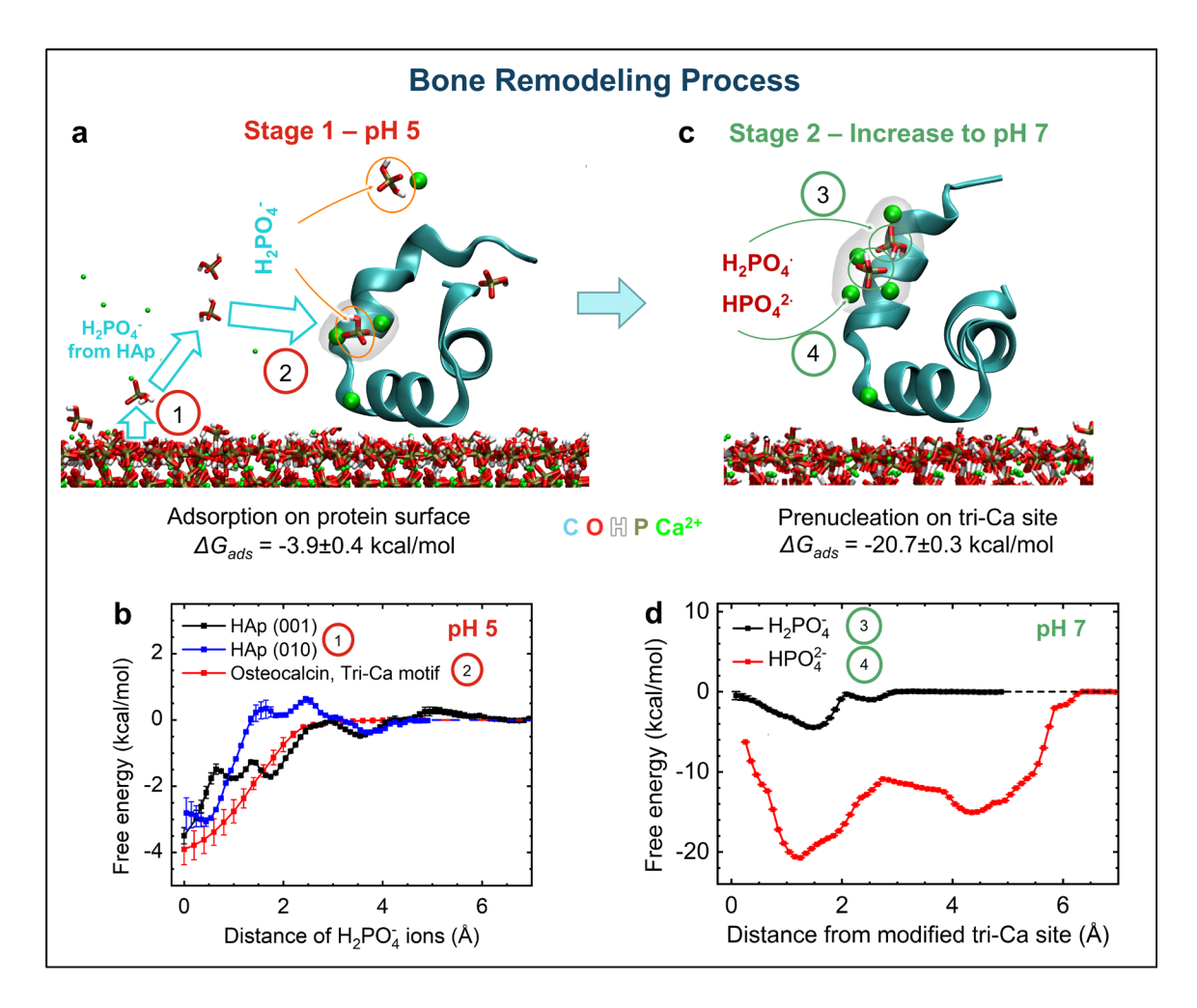


Figure 6. Pathway of bone remodeling at the molecular scale from pH 5 to pH 7, including free energy profiles for dissolution and precipitation of phosphate species. (a) The first stage of bone remodeling begins at pH 5. Dihydrogen phosphate ions partially dissolve from the HAp surfaces (Step 1) and osteocalcin binds to hydoxyapatite surfaces, illustrated for the (001) surface. Dihydrogen phosphate ions in solution adsorb preferentially onto the osteocalcin surface rather than onto the hydroxyapatite surface (Step 2), supported by a larger negative free energy difference (b). Protein-bound calcium ions and adsorbed dihydrogen phosphate ions are represented as solid spheres. (b) During the first stage of bone remodeling at pH 5, phosphate species (H₂PO₄⁻ ions) readily dissolve from the HAp surface due to relatively weak binding of ca. -3 kcal/mol (Step 1). The same phosphate species in solution show somewhat stronger adsorption of ca. -4 kcal/mol

onto the tricalcium site and the osteocalcin surface (Step 2). The free energy differences (also called potential of mean force) were obtained by steered molecular dynamics simulations. (c) The second stage of bone remodeling involves an increase in pH value from 5 to 7 and results in stronger adsorption of further protonated phosphate ions onto the initial prenucleation cluster near the tricalcium motif of osteocalcin (Steps 3 and 4). The phosphate species are now a mixture of HPO₄²⁻ and H₂PO₄⁻ ions. Hereby, the newly formed HPO₄²⁻ ions (step 4) adsorb much stronger than the existing H₂PO₄ ions (Step 3). Calcium and phosphate ions are represented by solid spheres. (d) Free energies of adsorption of individual HPO₄²⁻ and H₂PO₄⁻ ions onto the modified tricalcium site on the protein surface at the second stage of the remodeling process at pH 7. The binding free energy of HPO₄²⁻ ions of ca. -20 kcal/mol onto the existing prenucleation clusters is more than 15 kcal/mol stronger (Step 4) compared to the binding free energy of H₂PO₄ ions of ca. -4 kcal/mol. The difference explains the increased average attraction of phosphate species onto the protein structure at pH 7 in Stage 2, leading to calcium phosphate growth onto existing prenucleation clusters. The reference state are phosphate species in solution away from the protein surface.

Changes in Protein Function at pH 7 and Mechanism of Crystal Growth. At pH values of 7 and above, the adsorption of protonated phosphate ions onto bare Gla domains and onto the native protein becomes unfavorable (Figures 5d, Figure 7a). We exposed the equilibrium conformation of the native protein after adsorption on the HAp surface at pH 7 to a mixture of several dihydrogen phosphate, monohydrogen phosphate and calcium ions in the simulation (Figure 5d). In four out of five simulations, no phosphate species adsorbed on the tri-calcium motif of the protein. Instead, the monohydrogen phosphate ions and calcium ions formed stable tri- and

di-calcium bis(monohydrogen phosphate) pre-nucleation clusters in solution (Figures 5d, Figure 7b),²⁹ which also showed no adsorption to the osteocalcin surface. Repulsion from the protein was hereby higher for the positively charged Ca₃(HPO₄)₂²⁺ cluster than for the electroneutral Ca₂(HPO₄)₂ cluster. In addition, we also tested that substitution of calcium ions with twice the molar amount of Na⁺ ions (or addition of NaCl electrolyte) prevents the formation of the prenucleation clusters in aqueous solution and sustained a low probability of adsorption of monohydrogen phosphate ions onto the tri-calcium motif of osteocalcin.

The formation of prenucleation clusters of dihydrogen calcium phosphate was not observed across the pH range from 5 to 7 related to a higher solubility than calcium monohydrogen phosphate. The desorption free energies of monohydrogen phosphate ions from di- and tricalcium bis(monohydrogen phosphate) pre-nucleation clusters relative to desorption from the Gla domain on the native osteocalcin surface corroborate less attraction to osteocalcin (Figure 7c). Therefore, the native osteocalcin at pH values of 7 and above no longer plays a significant role in growing new prenucleation clusters. The free energy profile of pulling off a HPO₄²⁻ ion from the prenucleation clusters (Figure 7c) further shows a larger negative free energy of formation for the tri-calcium bis(monohydrogen phosphate) than for the di-calcium bis(monohydrogen phosphate), in support of a trend of cluster growth in solution. Furthermore, at pH 7, dissolution of calcium phosphate species from the hydroxyapatite surfaces is reduced compared to pH 5.

Accordingly, the role of osteocalcin changes at pH values of 7 or above, discontinuing the nucleation of new bone mineral. At the same time, growth of existing calcium phosphate nuclei on the tricalcium motif remains favorable. For further support of this hypothesis, we tested the possibility of reverse mineralization (Figure S3 in the Supporting Information). Forced removal of HPO₄²⁻ ions from the protein surface after remodeling (Figure S3a in the Supporting Information)

and from tricalcium bis(monohydrogen phosphate) clusters in solution at pH 7 (Figure S3b in the Supporting Information) shows stronger adhesion to the protein surface with a value of -20 kcal/mol than adhesion to prenucleation clusters in aqueous solution of only -13.5 kcal/mol (Figure S3c in the Supporting Information). Thus, binding of monohydrogen phosphate ions is stronger to calcium phosphate clusters attached to the tri-calcium site of osteocalcin than binding to prenucleation clusters in solution, supporting sustained growth of calcium phosphate nuclei attached to the protein surface at pH 7.

A second function of osteocalcin at pH 7, in addition to supporting the growth of new HAp clusters and crystals after remodeling, is the delay of the growth of HAp crystals where osteocalcin is adsorbed. The attraction of osteocalcin to several HAp surfaces (Figure 4e-g) remains significant at pH 7, even though weaker than at pH 5. Adsorbed osteocalcin, especially on prismatic (010) planes and (101) planes, continues to limit precursor access to these surfaces and thus delay their growth relative to osteocalcin-free systems.

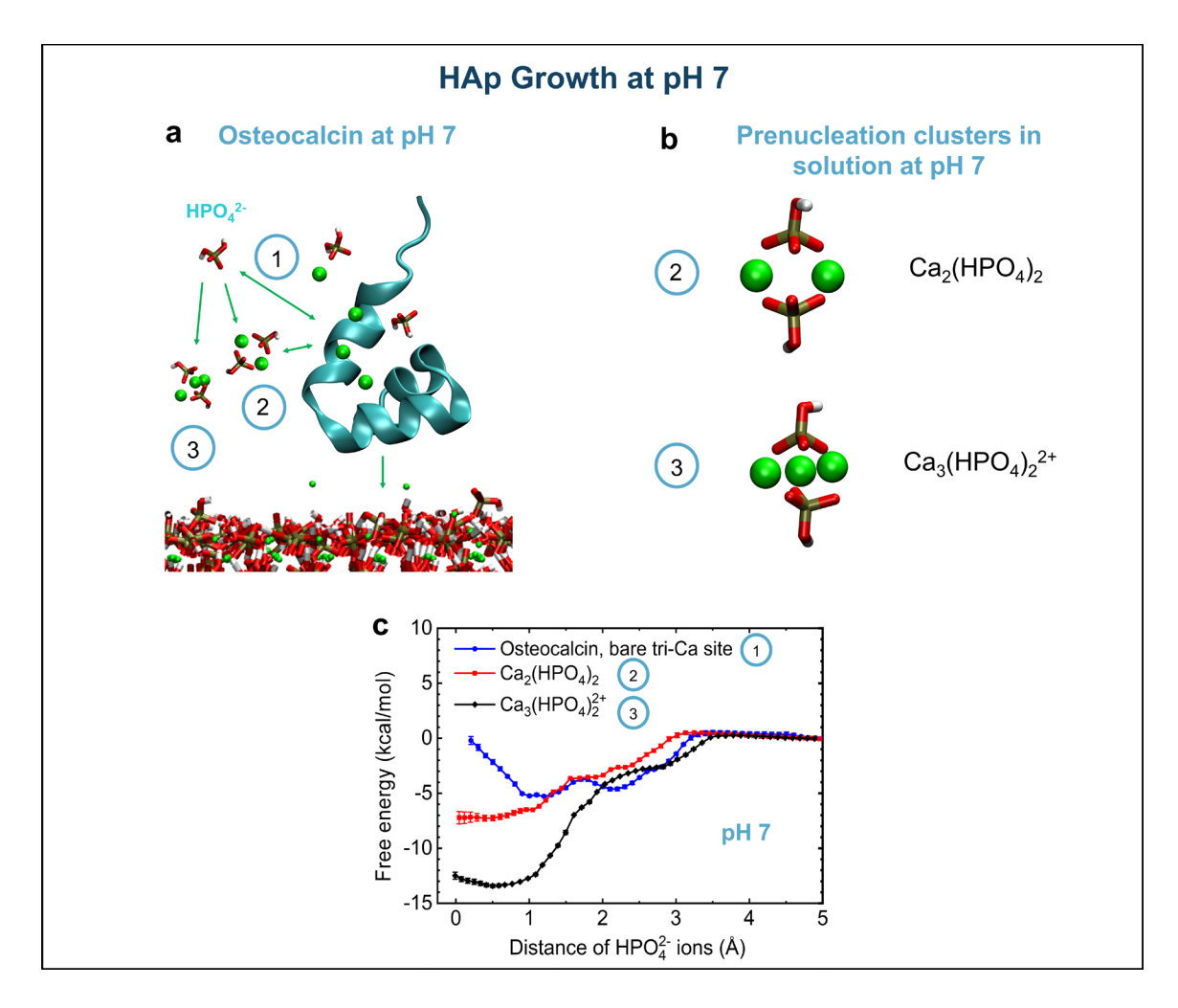


Figure 7. Role of osteocalcin in delaying HAp growth at pH 7. HAp growth at pH 7 involves the formation of prenucleation clusters in solution rather than on the surface of osteocalcin in the native structure, or on its Gla domain. Osteocalcin binds to HAp surfaces and slows down HAp growth. Species in solution include a mixture of HPO₄²⁻ and H₂PO₄⁻ ions. (a) Schematic of nucleation at pH 7. Calcium and phosphate species have less affinity to the native protein surface (Step 1) than to prenucleation clusters in solution (Steps 2 and 3). (b) Structures of stable prenucleation clusters of dicalcium monohydrogen phosphate and tricalcium monohydrogen phosphate in solution at pH 7. Calcium ions are represented as green spheres. (c) The free energy profiles of adsorption of HPO₄²⁻ ions onto the bare tricalcium site of native osteocalcin (Step 1) versus free energy profiles of adsorption of HPO₄²⁻ ions onto the prenucleation clusters

Ca₂(HPO₄)₂ and Ca₃(HPO₄)₂²⁺ at pH 7 (Steps 2 and 3). The HPO₄²⁻ ions have a clearly lower affinity of binding to osteocalcin than to the prenucleation clusters, showing that native osteocalcin at pH 7 does not promote nucleation of new calcium phosphate. Step 1 is therefore not preferred, and Steps 2 and 3 contribute to HAp growth.

Implications for the Role of Osteocalcin. The insights into osteocalcin function from molecular simulation and the known experimental information (X-ray structure, pK data, binding trends, observed conditions for bone remodeling and crystal growth) suggest a dual role. (1) Osteocalcin promotes new HAp growth starting at slightly acidic conditions at a pH value near 5 and supports calcium phosphate cluster growth as the pH value increases back to 7, partly driven by changes in protein structure and surface charge upon changing to an acidic pH value. (2) Osteocalcin delays HAp growth by adsorption onto (hkl) surfaces at both lower pH values of 5 as well as in the native structure at physiological pH values of 7, then with somewhat reduced strength relative to pH 5. Importantly, the simulations mimic in vivo conditions starting with bone remodeling at pH 5 and ending at pH 7 whereas typical in vitro studies to-date have considered pH 7 for bone growth.

The proposed mechanism explains the findings of a number of prior studies (Table 1).^{5-11, 14-17, 46, 47} Namely, it has been reported that there is one osteocalcin protein for each HAp grain, ^{8, 48} which implies that osteocalcin either arrests bone growth or acts as a seed for new grains (#1 in Table 1). This observation is consistent with the prenucleation near the Gla domain, of which there is exactly one per osteocalcin molecule. Decarboxylation of osteocalcin slows down bone resorption and bone formation, ¹¹ which concurs with the proposed mechanism of nucleation and growth through the protein tricalcium motif, which contains the critical carboxylate groups (#2 in

Table 1). We have identified adsorption of dissolved dihydrogen phosphate to the tricalcium motif, containing the dual carboxylic acid groups, at pH 5 due to a charge imbalance (Figure 5b and Figure 6a, b) and favorable growth to prenucleation sites during the transition from pH 5 to pH 7 (Figure 5c and Figure 6c, d). The positive charge of tricalcium bis(monohydrogenphosphate) clusters in solution may also support attachment to existing prenucleation clusters on the osteocalcin surface during the transition from pH 5 to pH 7 and thereafter. In this manner, osteocalcin promotes nucleation and may grow new HAp by cluster attachment, facilitating and accelerating the initial stages of bone remodeling.

Osteocalcin was found to be absent in the first stage of the bone mineralization, ¹⁴ which is consistent with a function as an inhibitor of bone growth and as a seed for a new bone grain (#3 in Table 1). Osteocalcin inhibited the HAp crystallization (#4)⁵ or decreased the crystal growth rate at pH values near 7 (#5).⁶ Newer findings of osteocalcin expression in osteoblasts at late stages of mineralization have corroborated this idea (#6).⁴⁶ In the simulation under physiological conditions of pH 7, the protein adsorbs onto the prismatic HAp (010) surface, and partly onto other (hkl) surfaces, reducing the accessible area for ion deposition and growth (Figure 2). The screened positive charge of the calcium ions on the Gla domain and the electrostatic repulsion of tri-calcium bis(monohydrogen phosphate) clusters in the solution prevent significant adsorption of new ions onto the protein and nucleation at pH 7. Our molecular observations explain the inhibitor effect of osteocalcin on HAp growth at physiological pH of ~7 in these earlier studies.^{5-9, 46, 47}

The observation of shorter remodeling periods in the presence of osteocalcin (#7), the presence in the bone remodeling compartment (#8), and the absence in enamel that undergoes no remodeling (#9)^{10, 14-17} are also consistent with the proposed formation of new nuclei and clusters in the bone remodeling process from pH 5 to pH 7. Our study therefore links the function of osteocalcin as a

promoter of the remodeling process and an inhibitor of the growth of bone to a molecular mechanism and specific roles of amino acids in the protein sequence. The insights can be utilized towards protein modification, mineralization control, as well as potential cures for bone-related diseases and further experimentation.

Table 1. Prior experimental findings on the role of osteocalcin and the proposed explanation at the molecular level.

#	Earlier experimental observation	Ref	Explanation in the current work
1	One osteocalcin molecule is found in each HAp	8, 48	The Gla domain in osteocalcin
	grain in bone		acts as a seed for bone remodeling
2	The absence of osteocalcin causes a decrease in	11	Osteocalcin and the tricalcium site
	bone resorption and a more pronounced decrease		are necessary for new bone
	in bone formation		mineral nucleation
3	Osteocalcin is not present in HAp crystals in	14	Osteocalcin slows down and
	bone during the initial stage of growth and		interferes with growth of existing
	present in the fully mineralized crystal		HAp crystals at pH ~7 by
4	Osteocalcin inhibited the crystallization of HAp	5	adsorption via R20, E31, H35,
	at pH 7.3		R43, R44, A49, and other residues
5	Osteocalcin decreased the HAp growth rate	6	
6	Osteocalcin is expressed by osteoblasts at a late	46	
	stage of bio-mineralization		

7	Hard bone has 30 times more osteocalcin than	14, 16	Osteocalcin supports the
	spongy bone and shorter remodeling duration		formation of new nuclei and
	than spongy bone		clusters in the bone remodeling
8	Osteocalcin is present in the bone remodeling	17	process from pH 5 to pH 7
	compartment		
9	Enamel does not remodel and contains no	10, 15	
	osteocalcin or other Gla proteins		

Predictions from Computational Models and Proposed Molecular Mechanisms. Our main advance is the explanation of the bone remodeling processes from the molecular scale. The proposed mechanisms and data can be used to predict how remineralization mechanisms change and how binding of osteocalcin to HAp is affected and when we modify the protein, including the Gla domain and key residues, as well as the pH value and electrolyte conditions. The predictions can be tested as new experimental and clinical studies evolve.

Specifically, the pattern of binding residues of osteocalcin to hydroxyapatite can guide in targeted mutations of osteocalcin to modify binding to HAp and HAp crystal growth (Figure 4a). The modification of binding residues of osteocalcin at pH 5 such as 13-16, 27, 28, 31, 32, 35-38, 40, 43-45, 48 and 49 for less binding residues such as A, Y, and a C-protected neutral residue 49 would reduce binding to basal planes (001) of HAp and enhance crystal growth in the longitudinal direction (Figure 4a). The mutation of binding residues 1, 4, 13-15, 17, 18, 20, 21, 25-28, 31, 32, 35, 44, 48 and 49 to neutral, less binding residues could reduce binding to prismatic planes ((010) and (020)) of HAp and enhance crystal growth along the prismatic planes, decreasing the aspect ratio of crystallites. The suppression of HAp crystal growth by osteocalcin at pH values of 7 and

on (101) planes of HAp can be analogously reduced by modifying appropriate residues shown in Figure 4a. Vice versa, stronger adsorption and suppression of crystal growth may be reached by replacing nonbinding residues in osteocalcin (Figure 4a) by more binding residues such as D, E, H, R, or K. The data also show how differences in pH value and in (hkl) crystal facets (crystallite shape) can be utilized to amplify changes in binding using specific fingerprints of binding residues (Figure 4a-g).

The proposed molecular mechanism of bone remodeling (Figure 5) allows informed modifications of the binding site for Ca phosphate nucleation. Knowing the importance of the residues on the Gla domain, targeted mutations can be made to enhance mineralization behavior, e.g., by replacing U residues in select locations (shown in Figure 4a) with less calcium-binding residues or adding additional Gla residues. In addition, the key role of D30 and D34 in calcium nucleation at pH 5 could be selectively engineered (Figure 4a, Figure 5a, b). Such modifications can also affect crystallite size and structural characteristics of newly mineralized bone.

The sensitivity to specific pH values and quantitative trends in free energies of binding (Figures 5 and 6) can further guide kinetic studies of Ca phosphate mineralization in the presence of osteocalcin and facilitate estimates of the impact of different solution environments. The observed conformation changes of osteocalcin from pH 7 to pH 5 can guide the design of molecular blockers (drugs) for the Gla site that fit specific pH-dependent molecular geometries and could suppress remineralization activity (Figure 5a).

Conclusions

We present a molecular-level analysis of binding of osteocalcin to hydroxyapatite surfaces under physiological conditions and likely initial mechanisms of bone remineralization and hydroxyapatite growth during bone remodeling. We explain how osteocalcin both promotes growth of new bone starting at pH 5 and delays the growth of hydroxyapatite crystals at pH 7. Osteocalcin binds to hydroxyapatite, whereby binding residues depend on the pH value and crystallographic facets, with stronger binding observed at pH 5 than at pH 7. Key binding residues include the positively charged N-terminus K-1, P-13, D-14, E-31, H-35, R43 and R44, as well as the C-terminus A-49. The Gla domain with U residues U17, U21, and U24 changes protonation states from pH 5 to 7 and its affinity to binding of phosphate species depends on the acidity in the surrounding cellular fluid. The Gla domain does not bind to hydroxyapatite surfaces and remains exposed to solution to facilitate growth of new mineral nuclei.

At pH 5, dissolved dihydrogenphosphate species initiate nucleation of new calcium phosphate near the Ca binding sites on osteocalcin, which involve the Gla domain, D30 and D34. The structure of osteocalcin hereby departs from the native structure at pH 7 due to the changing positions of the Ca²⁺ ions and attached prenucleation clusters. The emerging Ca-phosphate prenucleation clusters grow larger upon an increase in pH value towards 7, which adds monohydrogenphosphate species with stronger binding as well as more negatively charged sites at the U residues that attract additional Ca²⁺ ions. Native osteocalcin at pH values near 7 is only marginally involved in nucleation of calcium phosphate compared to prenucleation in solution, and likely slows down hydroxyapatite growth due to the attraction of osteocalcin to the prismatic plane. The proposed mechanisms are supported by molecular dynamics simulations using previously validated models, free energy calculations, and extensive prior experimental observations of the effects of osteocalcin. The mechanistic insight can be used to genetically

engineer osteocalcin to modulate calcium and phosphate binding, the attraction to hydroxyapatite surfaces, design drugs that block the calcium phosphate nucleation sites, as well as to further interrogate and modify bone repair mechanisms from the molecular scale as experimental techniques in high resolution become available.

Computational Methods

Osteocalcin and Hydroxyapatite Models. The crystal structure of porcine osteocalcin from the Protein Data Bank (ID: 1q8h) was used as an all-atom model (Figure 1).³ The structure consists of 49 amino acids including 15 charged residues, three Ca²⁺ cations and further ions for charge neutrality (Figure 1a). The protein contains three non-essential amino-acids called γ-carboxyl glutamate (Gla), which are represented by "U" (Figure 1b). pKa values were calculated using the chemicalize web interface⁴⁹. pH values of 5 and 7 were represented by deprotonation of one and two carboxylate groups in the side chain of U, respectively.

The first 12 residues of osteocalcin have a random coil structure and were not included in the PDB file.³ We added these residues to the protein structure as a peptide with the correct amino-acid sequence, representing the complete amino acid sequence. Several simulations in water were carried out, and we chose the osteocalcin structure of lowest energy for subsequent simulations. The follow-on simulations showed that the presence of the N-terminal random coil section did not affect the role of the tri-calcium motif in the remodeling process (Figure S1). The role in binding to HAp is also limited, with some attraction of the N-terminus at pH 7 (Figure 4).

The models of the HAp surfaces were created using the Interface force field (IFF) surface model database, including common (hkl) facets and chemically realistic representations of the surface chemistry as a function of pH (Figure 1c, Figure 2).^{25, 27} Thereby, the bulk HAp chemistry

Ca₅(OH)(PO₄)₃ was modified by appropriate protonation and removal of calcium ions from the surface. The Materials Studio program⁵⁰ was used to build the HAp models, and IFF building tools were used to create models of the aqueous protein interfaces.²⁵

The simulations utilized the IFF-CHARMM36 force field, with IFF parameters applied to the mineral and ionic species²⁷ and CHARMM36 parameters applied to the protein.²⁸ IFF-CHARMM has earlier shown insight into specific molecular recognition,^{37, 51-53} crystal growth,^{54, 55} lipid and peptide binding to mineral surfaces in chemical accuracy,^{26, 35, 56-58} as well as apatite mineralization in collagen²⁹ and ion substitution in hydroxyapatite surfaces in excellent agreement with available experimental data.³³

Fixed-Charge versus Polarizable Force Fields. IFF and CHARMM36 used in this study employed fixed atomic charges, and sometimes questions about benefits of using polarizable potentials arise. The answers are tied to one major problem of most force fields other than IFF, which is the use of unphysical, incorrect principal atomic charges. ^{25, 59} IFF uses carefully validated principal atomic charges for diverse chemistries that quantitatively represent covalent and ionic contributions to bonding. This approach, along with interpretability of all parameters and validation against trustworthy experimental data leads to multiple times higher accuracy than DFT calculations and an order of magnitude higher accuracy than other force fields, including multivalent metal ions. ⁶⁰ Polarizability adds benefits when it plays a major role, e.g., for image charges in metals ³⁵ and π electrons in aromatic molecules. ³¹ It is not suited to offset incorrect principal atomic charges, and the actual amount of polarization of divalent metal ions in solution is only a secondary effect. For example, calcium ions in HAp and in solution are represented in IFF by an effective charge of +1.5e, which captures both ionic and covalent contributions to calcium-phosphate, calcium-water, and calcium-protein interactions. ²⁷

A shortcoming in prior modeling of divalent cations such as Ca^{2+} has been the assumption of formal charges of +2.0e, when in physical reality the atomic charge of Ca^{2+} ions is only between 1.3e in oxides⁶⁰ and 1.7e in hydrated structures such as gypsum and hydroxides.⁶¹ Coordination environments in proteins with carboxylate groups are expected to be similar to those in hydrogen phosphates and in sulfates, unlikely close to +2.0e, and coordination environments in water likely less ionic than in hydroxides, too. IFF considers the approximate polarization of Ca^{2+} ions in the models ($+1.5e\pm0.2e$), and we observed no signs of charge inversion on the protein surface as the total charge of adsorbed phosphate and calcium ions were the same. Hereby, also the HPO₄²⁻ ions follow consistent chemistry with a net charge of -1.5e.²⁷

Accordingly, polarization is a second order effect, which would describe local deviations from a meaningful median value and potentially reduce uncertainties. Unfortunately, polarizable force fields have sometimes been advertised as an improvement when the underlying assumptions about the principal atomic charges were incorrect (e.g., +2.0e instead of +1.5e±0.2e for Ca²⁺ in HAp). Added polarization will not fix these problems. The current status can also be seen from the implementation of phosphate species in CHARMM36 and earlier CHARMM versions, which carry unrealistically high charges of P of +1.6e, instead of +0.9e ±0.1e according to IFF and electron deformation densities from experimental measurements. Simulation results using these parameters, e.g., for phosphate buffers or nucleotides, with or without polarizable terms, have little predictive value.

In conclusion, the accurate physical representation of the principal atomic charges of Ca²⁺ ions is of primary importance and the inclusion of further polarization can add minor improvements. However, typical approaches such as adding a dummy electron as in core-shell models,⁶² using parameters from a polarizable force field with untested compatibility, or using reactive forcefields

such as ReaxFF⁶³ do not lead to reliable parameters for mineral-protein interfaces overall. Also, the derivation of interpretable, compatible polarizable models is very time-consuming and the validation/measurement of success relative to experimental data often unclear. Suitable experimental data or reliable high-level quantum mechanical data for validation may be difficult to identify, ambiguous, or unavailable. Therefore, decreasing or increasing the atomic charge of a metal ion and its counterion to accommodate the environment using chemical principles (or intuition) and available experimental data is often the best solution and the first choice in IFF.

HAp Protein Interactions. For the two different pH values of 5 and 7, the interactions of osteocalcin with the (001), (010) and (101) facets of HAp were investigated using initial parallel and perpendicular orientations of osteocalcin at a physiological temperature of 310 K and atmospheric pressure of 101.3 kPa (Figure 1c and insets in Figure 3a, b, g, h). The perpendicular orientations tested specifically the possible role of the tri-calcium motif in adsorption as then the calcium ions faced toward the surface. The initial configurations assumed a minimum distance of 5 Å of the protein from the HAp surface, which was previously shown to be effective for conformation sampling. 55, 64

The model systems contained approximately 50,000 explicit TIP3P water molecules, enabling a water cushion of at least 4 nm thickness in the z direction. The size of the simulation box was equal to the HAp dimensions in x and y directions to emulate infinite HAp surfaces. Na⁺ and Cl⁻ ions with a concentration of 150 mM were added to mimic physiological conditions in the human body. The simulation boxes had a typical size of 8x7x11 nm³.

The osteocalcin binding simulations were carried out in several stages. First, an energy minimization of 500 steps and equilibration of 0.5 ns were utilized to relax the protein and HAp structures and remove initial close contacts. During these steps, the bottom layer of HAp with a

thickness of 2 Å and the backbone atoms of the protein were harmonically constrained. Subsequently, the constraints on the backbone atoms were removed and molecular dynamics (MD) simulations carried out for a period of 60 ns. The configuration of the system after 60 ns duration of the simulation was used to test the reproducibility of the simulation results. Using this configuration, four or five replicas with different protein-HAp distances were built. Keeping the constraint on the lower layer of the HAp, at least 7 ns of MD simulations were carried out for each replica. All simulations utilized the NPT ensemble (constant temperature and pressure) and the NAMD program. Langevin pressure and temperature control algorithms were employed. A spherical cutoff of 12 Å was used for Lennard-Jones interactions (standard in IFF and very similar to CHARMM), and the electrostatic interactions were treated in high accuracy of 10-6 with the PME method. Visualizations were carried out using the VMD program.

Calcium Phosphate Mineralization. The structure of the protein from the 60 ns simulation was deployed to test the possible role of the calcium ions in the bio-mineralization process. To lower the computational cost, the HAp surface was removed from the system and the contact residues were restrained. A typical box dimension was 5.5x5.5x5.5 nm³. Three or four dihydrogen or monohydrogen phosphate ions were placed in random positions inside the simulation box containing the protein, as well as Ca²⁺ ions and Cl⁻ ions to maintain charge neutrality. The potential energy of the system was recorded to monitor convergence to equilibrium, which is equivalent to monitoring the total energy as the kinetic energy/temperature was held constant. The potential energies were averaged using blocks of 1 ns length using the same simulation protocol as above.

For the computation of the adsorption free energy of the ions on the tri-calcium motif of the protein, several initial configurations with ions in random positions in the proximity of the protein were tested (Figures 6 and 7). The average adsorption free energy of each system was reported

along with the standard error (defined as the standard deviation of values divided by the square root of the number of simulations).

Steered Molecular Dynamics (SMD) Simulations. SMD simulations were used to calculate the adsorption free energies of the phosphate ionic species on the protein in the prenucleation process (Figure 6b, 6d, 7c, Figure S2, and Figure S3). For each free energy calculation, between 60 and 100 non-equilibrium SMD simulations were performed to sample the non-equilibration work parameter and obtain a Gaussian distribution.⁶⁷ In each SMD simulation, a spring with a stiffness of 210 to 1470 kcal/mol/Å² was used to pull a phosphate-type ion ($H_2PO_4^-$ or HPO_4^{2-}) with a velocity of 1 Å/ns away from the protein in a direction perpendicular to the tri-calcium motif, and the typical duration of each replica was 60 ns. The ion was initially in the equilibrium position (as obtained before). As opposed to pulling the ions towards the surface, the pulling-away path avoids unstable positions. The Jarzynski equation was deployed to calculate the free energy profile ΔG :^{67, 68}

$$e^{-\beta\Delta G} = \langle e^{-\beta W} \rangle \tag{1}$$

Thereby, ΔG is the free energy difference between the state with phosphate species adsorbed on the protein surface minus the state in which the phosphate species is very far from the surface, $\beta = 1/(RT)$, W is the work of the spring, and the edged brackets represent the ensemble average over multiple simulations.^{67, 68}

For the free energy calculations (Figure 6b, d), we utilized the osteocalcin structure from the protein database at pH 7, changed the protonation state corresponding to a pH value of 5, and let the protein adsorb onto HAp. Subsequently, phosphate and calcium ions absorbed onto the protein surface, providing initial structures for the free energy calculations at pH 5 (Figure 6b). Then, the

pH value and the corresponding protonation states were adjusted back to 7, providing initial structures for the calculations at pH 7 (Figure 6d).

For the calculations of the attraction of HPO₄⁻ ions to the prenucleation clusters at pH 7 and to osteocalcin, the entire native protein was used (Figure 7c). Among the many simulation replicas obtained, in one of them a HPO₄⁻ ion was adsorbed onto the tri-Ca site of the native protein. This final structure was utilized for the free energy calculation (blue curve in Figure 7c). In all other simulations, prenucleation clusters were formed in solution and used for analysis of HPO₄⁻ attraction (Figure 7c and Figure S3 in the Supplementary Information).

Reliability and Limitations. A common limitation in all-atom simulations is the finite number of atoms. In this work, we are restricted to domains of ~10 nm size in explicit electrolyte and a timescale of several microseconds. The scale is sufficient to examine molecular mechanisms, however, we have not examined hierarchical multiscale processes in bone remineralization.

The force field parameters for the calcium phosphate species, HAp, and osteocalcin have minor errors. Surface and hydration energies agree approximately within ±10% of experimental measurements and extensive validation is available.²⁵⁻³³ Reported binding energies and free energies during bone remodeling are expected to be of similar reliability. The assumption of protonation states of HAp surfaces, phosphate species, and protein residues according to pK values has a major influence on the results and is well supported by experimental data.^{25, 27} An open question is hereby the thickness of the protonated phosphate layer on the hydroxyapatite surfaces. We assume a thickness of one molecular layer, and multiple molecular layers might also be considered in future studies. Polarizability of ions and functional groups can play an additional role, however, using theoretically and experimentally well supported principal atomic charges in

IFF and CHARMM36 leads to several times higher accuracy than using less interpretable force fields with additional empirical polarization terms.

To validate the reproducibility of the results for protein adsorption on the HAp (hkl) surfaces, the contact residues in each replica were identified. The similarity of the contact residues among all replicas of MD simulations of 60 ns duration was used as a measure for uncertainty and found to be very high, nearly identical.

The free energy calculations include two main sources of errors, statistical error and sampling error through a finite number of replicas. The statistical error in free energies was derived from the standard error of $e^{-\beta W}$ for all trajectories, using error propagation analysis of equation (1):

$$\delta(\Delta G) = \left| -\frac{\delta(e^{-\beta W})}{\beta \langle e^{-\beta W} \rangle} \right| \tag{2}$$

and found to be in the low percent range. The sampling error, as a further contribution, decreases with lower pulling velocity in steered molecular dynamics and with a higher number of replicas. We demonstrated in a recent prior study that a pulling speed of 1 Å/ns and 10 to 30 replicas were sufficient to achieve convergence of binding free energies of amino acids and highly charged citrate ions onto dynamically reconstructing hydroxyapatite surfaces with ~10% uncertainty.³² Here, we used the same pulling speed of 1 Å/ns and 60 to 100 replicas, which is expected to lower the sampling errors to a range of 5% to 10%, and corresponds to between 3 and 6 μ s total simulation time for each system. More broadly, the sampling error depends on the pulling velocity, the number of runs N, and on the entropy change ΔS through the term $Nexp(\Delta S/k_B)$. Park and Schulten reported errors of ~50% and ~5% for pulling speeds of 100 Å/ns and 10 Å/ns, respectively, for the unfolding of a protein with 100 trajectories.⁶⁹ In comparison, we used a much slower pulling speed of 1 Å/ns with 60 to 100 replicas, consistently suggesting a sampling error below 5%. The entropy change ΔS in our SMD simulations of removing ions from the surfaces of

the osteocalcin, hydroxyapatite, or prenucleation clusters is close to zero or slightly negative.³³ We verified that the slow pulling speed with 60 to 100 trajectories was sufficient for convergence and a cumulative uncertainty of free energy calculations on the order of 10%, including both statistical and sampling errors.^{32, 70-73, 74}. Umbrella sampling offers an alternative to SMD to obtain free energies profiles for the forced motion of a molecule and could better accommodate the mobility of water, as well as somewhat improve the convergence and resolution relative to SMD.^{32, 71, 72, 75} A verified uncertainty of ~10% is acceptable, however, whether obtained via SMD or umbrella sampling.

Acknowledgements

We acknowledge support from the National Science Foundation (DMREF 1623947, CBET 1530790, OAC 1931587, DMREF 2323546) and the University of Colorado Boulder. M. T. acknowledges additional support from the Iranian ministry of science, research and technology, and from the Iranian national elite foundation. The allocation of computational resources at the Argonne Leadership Computing Facility, which is a DoE Office of Science User Facility supported under contract no. DE-AC02-06CH11357, and the Summit supercomputer at CU Boulder, which is supported by the National Science Foundation (award number ACI 1532235 and ACI 1532236) are acknowledged.

Declaration of Interests

The authors declare no competing interests.

Supporting Information Available

Additional Figures of hydroxyapatite surface chemistry as a function of pH, osteocalcin interaction with the hydroxyapatite surface, stabilization of the non-native osteocalcin structure upon increase in pH value from 5 to 7, desorption of phosphate species from prenucleation clusters formed on the osteocalcin surface versus prenucleation clusters in solution; additional text including details of osteocalcin binding to hydroxyapatite surfaces, calcium phosphate nucleation, and key findings; coordinate files, raw and processed simulation data, force field files, and simulation scripts to reproduce the results.

References

- 1. Rosenquist, C.; Qvist, P.; Bjarnason, N.; Christiansen, C., Measurement of a More Stable Region of Osteocalcin in Serum by ELISA With Two Monoclonal Antibodies. *Clin. Chem.* **1995**, *41*, 1439-1445.
- 2. Chenu, C.; Colucci, S.; Grano, M.; Zigrino, P.; Barattolo, R.; Zambonin, G.; Baldini, N.; Vergnaud, P.; Delmas, P. D.; Zallone, A. Z., Osteocalcin Induces Chemotaxis, Secretion of Matrix Proteins, and Calcium-Mediated Intracellular Signaling in Human Osteoclast-Like Cells. *J. Cell. Biol.* **1994**, *127*, 1149-1158.
- 3. Hoang, Q. Q.; Sicheri, F.; Howard, A. J.; Yang, D. S. C., Bone Recognition Mechanism of Porcine Osteocalcin from Crystal Structure. *Nature* **2003**, *425*, 977-980.
- 4. Ducy, P.; Desbois, C.; Boyce, B.; Pinero, G.; Story, B.; Dunstan, C.; Smith, E.; Bonadio, J.; Goldstein, S.; Gundberg, C.; Bradley, A.; Karsenty, G., Increased Bone Formation in Osteocalcin-Deficient Mice. *Nature* **1996**, *382*, 448-452.
- 5. Price, P. A.; Otsuka, A. A.; Poser, J. W.; Kristaponis, J.; Raman, N., Characterization of a Gamma-Carboxyglutamic Acid-Containing Protein from Bone. *Proc. Nat. Acad. Sci. USA* **1976,** *73*, 1447-1451.
- 6. Romberg, R. W.; Werness, P. G.; Riggs, B. L.; Mann, K. G., Inhibition of Hydroxyapatite Crystal Growth by Bone-Specific and Other Calcium-Binding Proteins. *Biochemistry* **1986**, *25*, 1176-80.
- 7. Boskey, A. L.; Wians, F. H.; Hauschka, P. V., The Effect of Osteocalcin on In vitro Lipid-Induced Hydroxyapatite Formation and Seeded Hydroxyapatite Growth. *Calcified Tissue Int.* **1985**, *37*, 57-62.
- 8. Poser, J. W.; Price, P. A., A Method for Decarboxylation of Gamma-Carboxyglutamic Acid in Proteins. Properties of the Decarboxylated Gamma-Carboxyglutamic Acid Protein from Calf Bone. *J. Biol. Chem.* **1979**, *254*, 431-436.

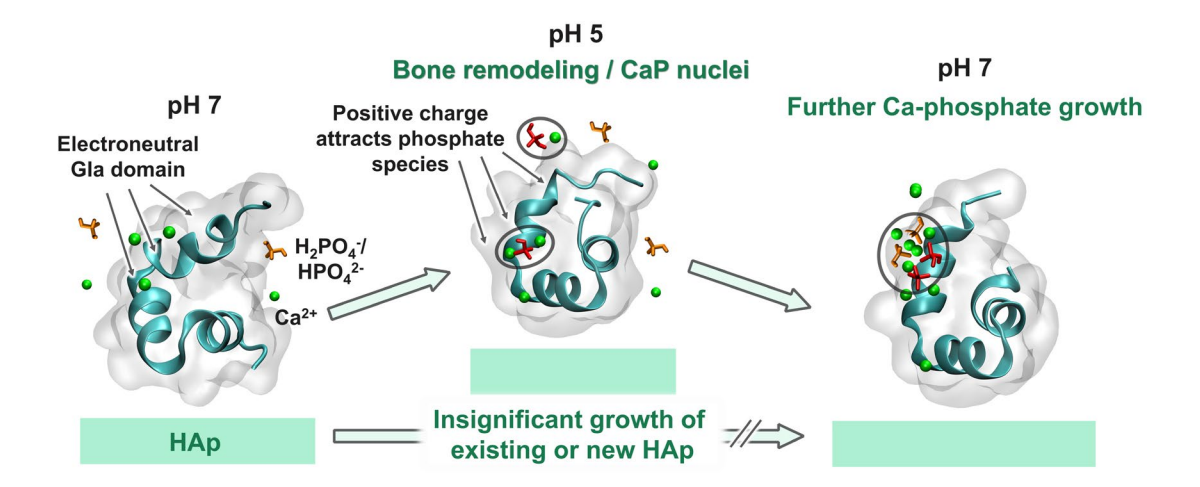
- 9. Hunter, G. K.; Hauschka, P. V.; Poole, A. R.; Rosenberg, L. C.; Goldberg, H. A., Nucleation and Inhibition of Hydroxyapatite Formation by Mineralized Tissue Proteins. *Biochem. J.* **1996**, *317* (*Pt 1*), 59-64.
- 10. Hauschka, P. V.; Reid, M. L., Timed Appearance of a Calcium-Binding Protein Containing Gamma-Carboxyglutamic Acid in Developing Chick Bone. *Developm. Biol.* **1978**, 65, 426-434.
- 11. Pastoureau, P.; Vergnaud, P.; Meunier, P. J.; Delmas, P. D., Osteopenia and Bone-Remodeling Abnormalities in Warfarin-Treated Lambs. *J. Bone Miner. Res.* **1993**, *8*, 1417-1426.
- 12. Black, D. M.; Rosen, C. J., Postmenopausal Osteoporosis. *New Engl. J. Med.* **2016,** *374*, 254-262.
- 13. Bandeira, F.; Vasconcellos, L. I. F.; Souza, L., Atypical Localization of Paget's Disease of Bone: A Case Series and Systematic Review of the Literature. *Int. J. Med. Rev. Case Rep.* **2020,** *4*, 49-56.
- 14. I., R. H., Why Does Bone Matrix Contain Non-Collagenous Proteins? The Possible Roles of Osteocalcin, Osteonectin, Osteopontin and Bone Sialoprotein in Bone Mineralisation and Resorption. *Cell Biol. Int.* **1994**, *18*, 617-628.
- 15. Moradian-Oldak, J., The Regeneration of Tooth Enamel. *Dimens Dent. Hyg.* **2009,** 7, 12-15.
- 16. Eriksen, E. F., Cellular Mechanisms of Bone Remodeling. *Rev. Endocrine Metabolic Disorders* **2010**, *11*, 219-227.
- 17. M., H. E.; Dorte, Q.; Fink, E. E.; Leif, M.; Flemming, M., Cancellous Bone Remodeling Occurs in Specialized Compartments Lined by Cells Expressing Osteoblastic Markers. *J. Bone Mineral Res.* **2001**, *16*, 1575-1582.
- 18. Parfitt, A. M., The Bone Remodeling Compartment: A Circulatory Function for Bone Lining Cells. *J. Bone Miner. Res.* **2001**, *16*, 1583-1585.
- 19. Andersen, T. L.; Sondergaard, T. E.; Skorzynska, K. E.; Dagnaes-Hansen, F.; Plesner, T. L.; Hauge, E. M.; Plesner, T.; Delaisse, J. M., A Physical Mechanism for Coupling Bone Resorption and Formation in Adult Human Bone. *Am. J. Pathol.* **2009**, *174*, 239-47.
- 20. Matsuo, K.; Irie, N., Osteoclast-Osteoblast Communication. *Arch. Biochem. Biophys.* **2008**, *473*, 201-9.
- 21. Clarke, B., Normal Bone Anatomy and Physiology. *Clin. J. Am. Soc. Nephrol.* **2008**, *3 Suppl 3*, S131-139.
- 22. Silver, I.; Murrills, R.; Etherington, D., Microelectrode Studies on the Acid Microenvironment Beneath Adherent Macrophages and Osteoclasts. *Exp. Cell Res.* **1988**, *175*, 266-276.
- 23. Ferron, M.; Wei, J.; Yoshizawa, T.; Del Fattore, A.; DePinho, R. A.; Teti, A.; Ducy, P.; Karsenty, G., Insulin Signaling in Osteoblasts Integrates Bone Remodeling and Energy Metabolism. *Cell* **2010**, *142*, 296-308.
- 24. Liu, L.; Schlesinger, P. H.; Slack, N. M.; Friedman, P. A.; Blair, H. C., High capacity Na+/H+ exchange activity in mineralizing osteoblasts. *J. Cell Physiol.* **2011**, *226*, 1702-1712.
- 25. Heinz, H.; Lin, T.-J.; Mishra, R. K.; Emami, F. S., Thermodynamically Consistent Force Fields for the Assembly of Inorganic, Organic, and Biological Nanostructures: The INTERFACE Force Field. *Langmuir* **2013**, *29*, 1754-1765.
- 26. Heinz, H.; Ramezani-Dakhel, H., Simulations of Inorganic–Bioorganic Interfaces to Discover New Materials: Insights, Comparisons to Experiment, Challenges, and Opportunities. *Chem. Soc. Rev.* **2016**, *45*, 412-448.

- 27. Lin, T. Z.; Heinz, H., Accurate Force Field Parameters and pH Resolved Surface Models for Hydroxyapatite to Understand Structure, Mechanics, Hydration, and Biological Interfaces. *J. Phys. Chem. C* **2016**, *120*, 4975-4992.
- 28. Huang, J.; MacKerell, A. D., CHARMM36 All-Atom Additive Protein Force Field: Validation Based on Comparison to NMR Data. *J. Comput. Chem.* **2013**, *34*, 2135-2145.
- 29. Ma, Y.-X.; Hoff, S. E.; Huang, X.-Q.; Liu, J.; Wan, Q.-Q.; Song, Q.; Gu, J.-T.; Heinz, H.; Tay, F. R.; Niu, L.-N., Involvement of Prenucleation Clusters in Calcium Phosphate Mineralization of Collagen. *Acta Biomater.* **2021**, *120*, 213-223.
- 30. Tanaka, H.; Chikazawa, M.; Kandori, K.; Ishikawa, T., Influence of Thermal Treatment on the Structure of Calcium Hydroxyapatite. *Phys. Chem. Chem. Phys.* **2000**, *2*, 2647-2650.
- 31. Akkineni, S.; Zhu, C.; Chen, J.; Song, M.; Hoff Samuel, E.; Bonde, J.; Tao, J.; Heinz, H.; Habelitz, S.; De Yoreo James, J., Amyloid-like Amelogenin Nanoribbons Template Mineralization via a Low-Energy Interface of Ion Binding Sites. *Proc. Natl. Acad. Sci. U. S. A.* **2022**, *119*, e2106965119.
- 32. Hoff, S. E.; Liu, J.; Heinz, H., Binding Mechanism and Binding Free Energy of Amino Acids and Citrate to Hydroxyapatite Surfaces as a Function of Crystallographic Facet, pH, and Electrolytes. *J. Colloid Interface Sci.* **2022**, *605*, 685-700.
- 33. Garley, A.; Hoff, S. E.; Saikia, N.; Jamadagni, S. N.; Baig, A. A.; Heinz, H., Adsorption and Substitution of Metal Ions on Hydroxyapatite as a Function of Crystal Facet and Electrolyte pH. *J. Phys. Chem. C* **2019**, *123*, 16982-16993.
- 34. Choi, Y. K.; Kern, N. R.; Kim, S.; Kanhaiya, K.; Afshar, Y.; Jeon, S. H.; Jo, S.; Brooks, B. R.; Lee, J.; Tadmor, E. B.; Heinz, H.; Im, W., CHARMM-GUI Nanomaterial Modeler for Modeling and Simulation of Nanomaterial Systems. *J. Chem. Theor. Comput.* **2022**, *18*, 479-493.
- 35. Geada, I. L.; Ramezani-Dakhel, H.; Jamil, T.; Sulpizi, M.; Heinz, H., Insight into Induced Charges at Metal Surfaces and Biointerfaces Using a Polarizable Lennard-Jones Potential. *Nat. Comm.* **2018**, *9*, 716.
- 36. Chen, J.; Zhu, E.; Liu, J.; Zhang, S.; Lin, Z.; Duan, X.; Heinz, H.; Huang, Y.; Yoreo, J. J. D., Building Two-Dimensional Materials One Row at a Time: Avoiding the Nucleation Barrier. *Science* **2018**, *362*, 1135-1139.
- 37. Emami, F. S.; Puddu, V.; Berry, R. J.; Varshney, V.; Patwardhan, S. V.; Perry, C. C.; Heinz, H., Prediction of Specific Biomolecule Adsorption on Silica Surfaces as a Function of pH and Particle Size. *Chem. Mater.* **2014**, *26*, 5725–5734.
- 38. Emami, F. S.; Puddu, V.; Berry, R. J.; Varshney, V.; Patwardhan, S. V.; Perry, C. C.; Heinz, H., Force Field and a Surface Model Database for Silica to Simulate Interfacial Properties in Atomic Resolution. *Chem. Mater.* **2014**, *26*, 2647-2658.
- 39. Hoff, S. E.; Di Silvio, D.; Ziolo, R. F.; Moya, S. E.; Heinz, H., Patterning of Self-Assembled Monolayers of Amphiphilic Multisegment Ligands on Nanoparticles and Design Parameters for Protein Interactions. *Acs Nano* **2022**, *16*, 8766-8783.
- 40. Ishikawa, T.; Wakamura, M.; Kondo, S., Surface Characterization of Calcium Hydroxylapatite by Fourier Transform Infrared Spectroscopy. *Langmuir* **1989**, *5*, 140-144.
- 41. Dowd, T. L.; Rosen, J. F.; Li, L.; Gundberg, C. M., The Three-Dimensional Structure of Bovine Calcium Ion-Bound Osteocalcin Using 1H NMR Spectroscopy. *Biochemistry* **2003**, *42*, 7769-7779.

- 42. Ivaska, K. K.; Hentunen, T. A.; Vaaraniemi, J.; Ylipahkala, H.; Pettersson, K.; Vaananen, H. K., Release of Intact and Fragmented Osteocalcin Molecules from Bone Matrix During Bone Resorption in Vitro. *J. Biol. Chem.* **2004**, *279*, 18361-18369.
- 43. Nelson, D. L.; Cox, M. M., *Lehninger Principles of Biochemistry*. 5th ed.; W.H Freeman and Company: New York, US, 2008.
- 44. Francis, M. D.; Webb, N. C., Hydroxyapatite Formation From a Hydrated Calcium Monohydrogen Phosphate Precursor. *Calcif. Tissue Res.* **1971**, *6*, 335-42.
- 45. Chow, L. C., Solubility of Calcium Phosphates. *Monogr. Oral Sci.* **2001**, *18*, 94-111.
- 46. Neve, A.; Corrado, A.; Cantatore, F. P., Osteocalcin: Skeletal and Extra-Skeletal Effects. *J. Cell Physiol.* **2013**, *228*, 1149-1153.
- 47. Boskey, A. L.; Gadaleta, S.; Gundberg, C.; Doty, S. B.; Ducy, P.; Karsenty, G., Fourier Transform Infrared Microspectroscopic Analysis of Bones of Osteocalcin-Deficient Mice Provides Insight into the Function of Osteocalcin. *Bone* **1998**, *23*, 187-96.
- 48. Hauschka, P. V.; Carr, S. A., Calcium-Dependent Alpha-Helical Structure in Osteocalcin. *Biochemistry* **1982**, *21*, 2538-47.
- 49. Swain, M., Chemicalize.org. J. Chem. Inf. Model. 2012, 52, 613-615.
- 50. *Materials Studio 7 Program Suite and User Guide*. Biovia/Dassault Systemes: Cambridge, UK, 2015-2019.
- 51. Heinz, H.; Castelijns, H. J.; Suter, U. W., Structure and Phase Transitions of Alkyl Chains on Mica. *J. Am. Chem. Soc.* **2003**, *125*, 9500-9510.
- 52. Heinz, H.; Farmer, B. L.; Pandey, R. B.; Slocik, J. M.; Patnaik, S. S.; Pachter, R.; Naik, R. R., Nature of Molecular Interactions of Peptides with Gold, Palladium, and Pd-Au Bimetal Surfaces in Aqueous Solution. *J. Am. Chem. Soc.* **2009**, *131*, 9704-9714.
- 53. Patwardhan, S. V.; Emami, F. S.; Berry, R. J.; Jones, S. E.; Naik, R. R.; Deschaume, O.; Heinz, H.; Perry, C. C., Chemistry of Aqueous Silica Nanoparticle Surfaces and the
- Mechanism of Selective Peptide Adsorption. J. Am. Chem. Soc. 2012, 134, 6244-6256.
- 54. Ruan, L. Y.; Ramezani-Dakhel, H.; Lee, C.; Li, Y. J.; Duan, X. F.; Heinz, H.; Huang, Y., A Rational Biomimetic Approach to Structure Defect Generation in Colloidal Nanocrystals. *Acs Nano* **2014**, *8*, 6934-6944.
- 55. Ramezani-Dakhel, H.; Ruan, L. Y.; Huang, Y.; Heinz, H., Molecular Mechanism of Specific Recognition of Cubic Pt Nanocrystals by Peptides and the Concentration-Dependent Formation from Seed Crystals. *Adv. Funct. Mater.* **2015**, *25*, 1374-1384.
- 56. Mishra, R. K.; Mohamed, A. K.; Geissbühler, D.; Manzano, H.; Jamil, T.; Shahsavari, R.; Kalinichev, A. G.; Galmarini, S.; Tao, L.; Heinz, H.; Pellenq, R.; Van Duin, A. C.; Parker, S. C.; Flatt, R. J.; Bowen, P., CEMFF: A Force Field Database for Cementitious Materials Including Validations, Applications and Opportunities. *Cem. Concr. Res.* **2017**, *102*, 68-89.
- 57. Schneemilch, M.; Quirke, N., Free Energy of Adhesion of Lipid Bilayers on Silica Surfaces. *J. Chem. Phys.* **2018**, *148*, 194704.
- 58. Schneemilch, M.; Quirke, N., Free Energy of Adsorption of Supported Lipid Bilayers From Molecular Dynamics Simulation. *Chem. Phys. Lett.* **2016**, *664*, 199-204.
- 59. Heinz, H.; Suter, U. W., Atomic Charges for Classical Simulations of Polar Systems. *J. Phys. Chem. B* **2004**, *108*, 18341-18352.
- 60. Kanhaiya, K.; Nathanson, M.; in 't Veld, P. J.; Zhu, C.; Nikiforov, I.; Tadmor, E. B.; Choi, Y. K.; Im, W.; Mishra, R. K.; Heinz, H., Accurate Force Fields for Atomistic Simulations

- of Oxides, Hydroxides, and Organic Hybrid Materials up to the Micrometer Scale. *J. Chem. Theor. Comput.* **2023**, *19*, 8293-8322.
- 61. Mishra, R. K.; Kanhaiya, K.; Winetrout, J. J.; Flatt, R. J.; Heinz, H., Force Field for Calcium Sulfate Minerals to Predict Structural, Hydration, and Interfacial Properties. *Cem. Concr. Res.* **2021**, *139*, 106262.
- 62. Mitchell, P. J.; Fincham, D., Shell-Model Simulations by Adiatabic Dynamics. *J. Phys. Condens. Mat.* **1993**, *5*, 1031-1038.
- 63. van Duin, A. C. T.; Dasgupta, S.; Lorant, F.; Goddard, W. A., ReaxFF: A Reactive Force Field for Hydrocarbons. *J. Phys. Chem. A* **2001**, *105*, 9396-9409.
- 64. Ramezani-Dakhel, H.; Bedford, N. M.; Woehl, T. J.; Knecht, M. R.; Naik, R. R.; Heinz, H., Nature of Peptide Wrapping onto Metal Nanoparticle Catalysts and Driving Forces for Size Control. *Nanoscale* **2017**, *9*, 8401-8409.
- 65. Phillips, J. C.; Braun, R.; Wang, W.; Gumbart, J.; Tajkhorshid, E.; Villa, E.; Chipot, C.; Skeel, R. D.; Kale, L.; Schulten, K., Scalable Molecular Dynamics with NAMD. *J. Comput. Chem.* **2005**, *26*, 1781-1802.
- 66. Humphrey, W.; Dalke, A.; Schulten, K., VMD Visual Molecular Dynamics. *J. Mol. Graphics* **1996**, *14*, 33-38.
- 67. Jarzynski, C., Nonequilibrium Equality for Free Energy Differences. *Phys. Rev. Lett.* **1997,** 78, 2690-2693.
- 68. Park, S.; Khalili-Araghi, F.; Tajkhorshid, E.; Schulten, K., Free Energy Calculation from Steered Molecular Dynamics Simulations Using Jarzynski's Equality. *J. Chem. Phys.* **2003**, *119*, 3559-3566.
- 69. Park, S.; Schulten, K., Calculating Potentials of Mean Force From Steered Molecular Dynamics Simulations. *J. Chem. Phys.* **2004**, *120*, 5946-5961.
- 70. Chipot, C.; Pohorille, A., Free Energy Calculation. Springer: New York, 2007.
- 71. Wang, S.; Zhu, E.; Huang, Y.; Heinz, H., Direct Correlation of Oxygen Adsorption on Platinum-Electrolyte Interfaces with the Activity in the Oxygen Reduction Reaction. *Sci. Adv.* **2021,** 7, eabb1435.
- 72. Wang, S.; Hou, K.; Heinz, H., Accurate Compatible Force Fields for Molecular Oxygen, Nitrogen and Hydrogen to Simulate Heterogeneous Electrolytes and Interfaces. *J. Chem. Theor. Comput.* **2021**, *17*, 5198-5213.
- 73. Jamil, T.; Javadi, A.; Heinz, H., Mechanism of Molecular Interaction of Acrylate-Polyethylene Glycol Acrylate Copolymers with Calcium Silicate Hydrate Surfaces. *Green Chem.* **2020,** *22*, 1577-1593.
- 74. Tavakol, M.; Vaughan, T. J., The Structural Role of Osteocalcin in Bone Biomechanics and its Alteration in Type-2 Diabetes. *Sci. Rep.* **2020**, 10, 17321.
- 75. Zhu, C.; Hoff, S. E.; Hémadi, M.; Heinz, H., Accurate and Ultrafast Simulation of Molecular Recognition and Assembly on Metal Surfaces in Four Dimensions. *Acs Nano* **2023**, *17*, 9938-9952.

Table of Contents Graphic



Supporting Information

for

Osteocalcin: Promoter or Inhibitor of Hydroxyapatite Growth?

Mahdi Tavakol,^{1,2} Juan Liu,¹ Samuel E. Hoff,¹ Cheng Zhu,¹ Hendrik Heinz^{1,3*}

¹ Department of Chemical and Biological Engineering, University of Colorado Boulder, 3415 Colorado Ave, Boulder, CO 80301, USA

² Department of Mechanical Engineering, Sharif University of Technology, PO Box 11365-

11155, Tehran, Iran

³ Materials Science and Engineering Program, University of Colorado Boulder, 3415 Colorado Ave, Boulder, CO 80301, USA

*Corresponding author: hendrik.heinz@colorado.edu

Table of Contents:

Supporting Figures S1 to S3

Supporting Text Sections S1 to S3

Supporting Reference

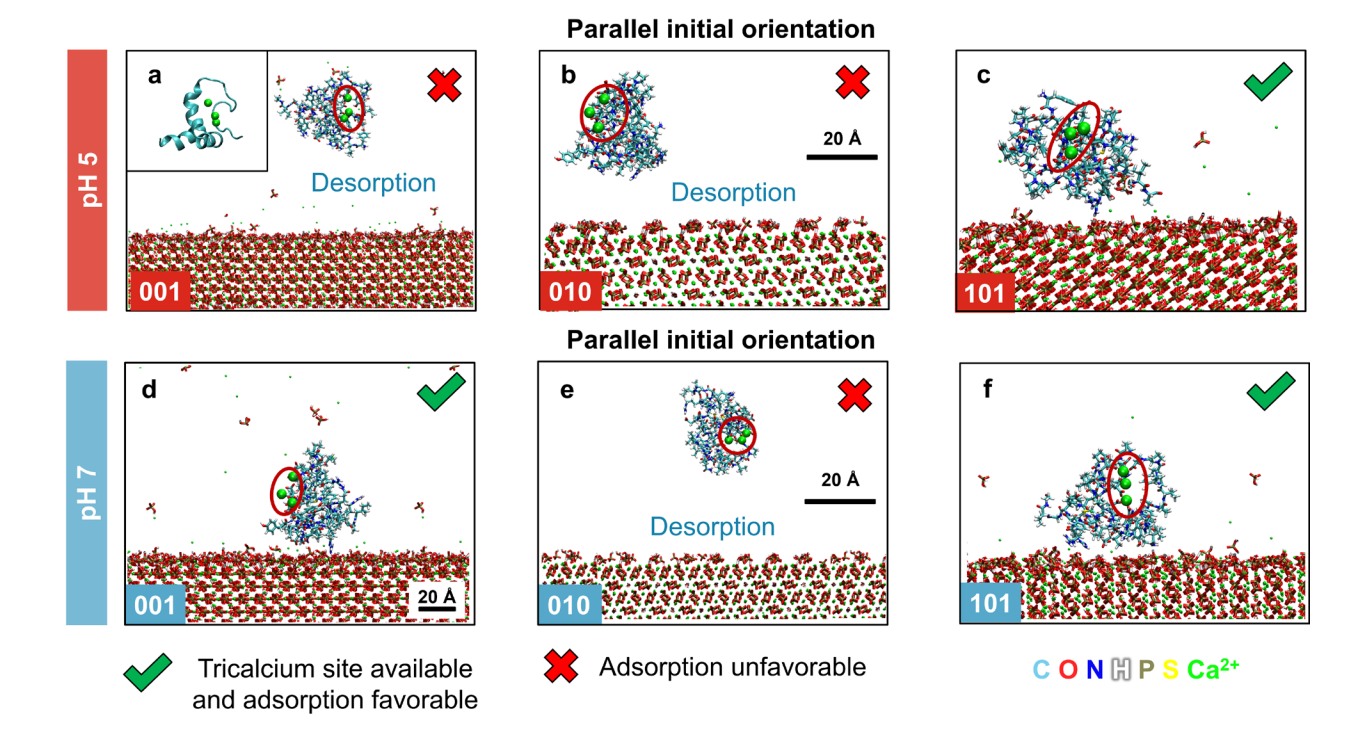


Figure S1. Additional snapshots of osteocalcin interacting with dominant hydroxyapatite (hkl) surfaces in equilibrium. The tricalcium motif remains exposed to the electrolyte solution and has no discernable affinity to hydroxyapatite surfaces (green spheres for the Ca²⁺ ions and red circular highlights). (a-c) Conformations on (001), (010), and (101) surfaces at pH 5, starting with parallel initial orientation (see inset in a). (d-f) Conformations on the same surfaces at pH 7 starting with parallel initial orientation. The snapshots are shown after ~10 ns simulation time and include both binding conformations and desorbed conformations.

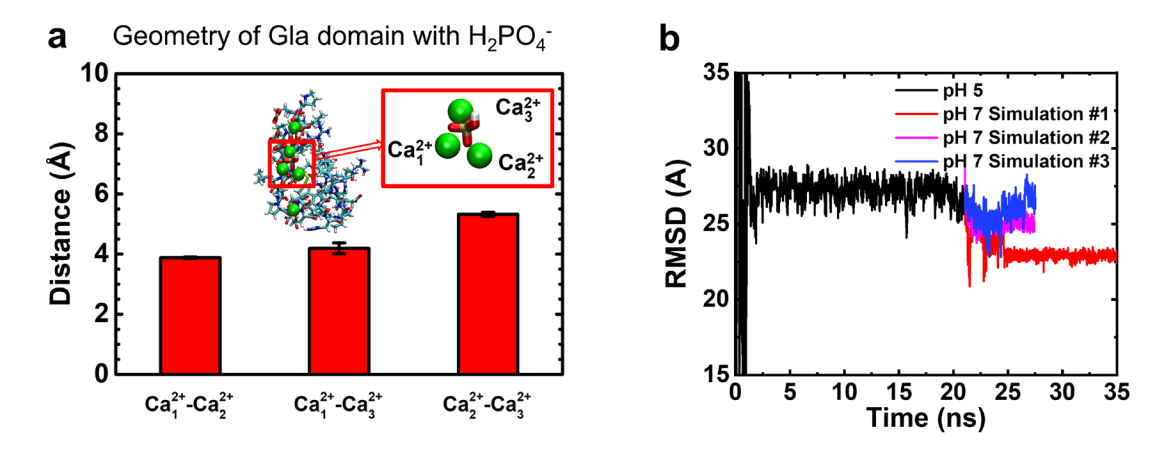


Figure S2. Stabilization of the non-native osteocalcin structure upon increase in pH value from 5 to 7 during bone remodeling. (a) Geometry and calcium-calcium distances at the Gla domain, containing one bound dihydrogenphosphate ion. Calcium ions bound to the surface of osteocalcin are shown as green spheres. (b) Root mean square displacement (RMSD) of the adsorbed dihydrogenphosphate ion and three surrounding calcium ions at the Gla domain. The increase in pH value to 7 lowers the mobility (RMSD) of the cluster, showing an increase in structural stability.

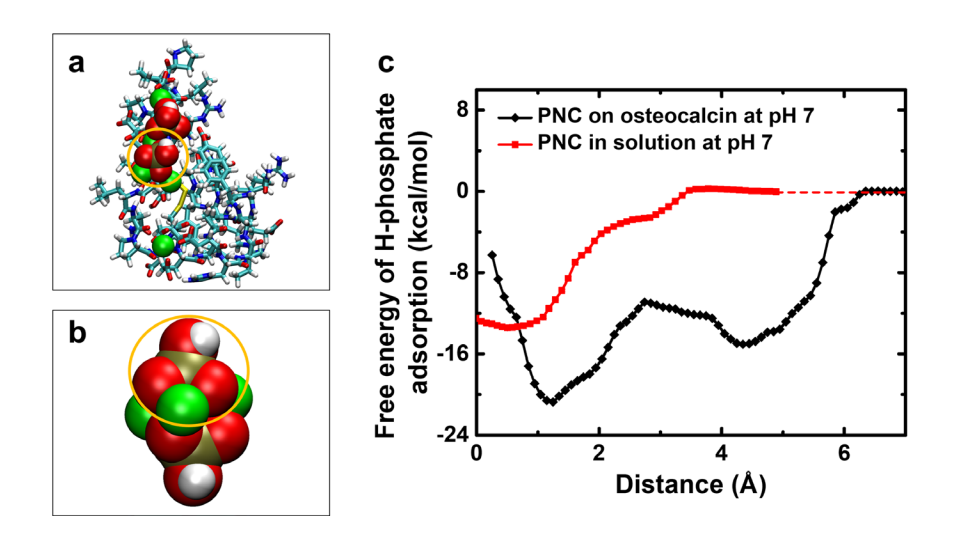


Figure S3. Desorption of phosphate species from prenucleation clusters (PNCs) formed on the osteocalcin surface during the remodeling process versus PNCs formed in solution at pH = 7. Binding is stronger in the PNCs on the osteocalcin surface. (a) The structure of osteocalcin with a surface-bound PNC after the remodeling process (yellow circle highlights phosphate ion chosen in steered MD simulations). (b) An energetically favorable calcium bis(monohydrogen phosphate) PNC formed in solution (yellow circle indicates phosphate ion chosen in steered MD simulations). (c) The desorption free energies of monohydrogen phosphate ions from the PNCs in (a) and (b). The reaction coordinate was perpendicular to the tri-calcium plane.

S1. Additional Details of Osteocalcin Binding to Hydroxyapatite Surfaces

At a pH value of 5, helix #1 binds mainly through P13 and D14, helix #2 through D28, E31, as well as H35, and helix #3 through R43 and R44. The N-terminus (K1) and, more intensely, the C-terminus (A49) are among the contact residues due to the charge and the flexibility of random coil sections of the protein (Figure 1a and Figure 4a). Arginine binds using the positive charge on the guanidinium side group through the formation of ion pairs with negatively charged hydrogen phosphate groups on the HAp surface, aided by the conformational flexibility of the R side chains and the ability to form additional hydrogen bonds with hydrogen phosphate ions. Binding of histidine (H35) involves similar interactions as arginine, especially in the protonated state at pH 5. Glutamate contributes to binding via negatively charged carboxylate groups and formation of ion pairs with calcium ions on the HAp surface, whereby longer side chains than in aspartate lead to more flexible, stronger binding.

At pH 5, the Gla residues only partially compensate the Ca²⁺ charge (Figure 1b and Figure 5a) and protein adsorption remains stronger via the residues near the N-terminus (Figure 3a, c, e), as well as D14 (Figure 3b, d and Figure 4) for α-helix #1. Stronger adsorption of these residues, supported by longer, flexible side chains, prevents the tri-calcium motif from significant adsorption onto the HAp surface. Intermittently, the negatively charged U17 residue in the Gla domain also serves as a contact residue to superficial calcium ions. At pH 7, the electrical charge of three calcium ions bound to the protein is fully screened by the two COO⁻ groups of each of the three Gla residues (Figure 5a), resulting in negligible electrostatic interactions between the HAp surface and the tricalcium motif.

The Gla domain with the tricalcium site plays a critical role for the function of osteocalcin. The U side chains can hold up to two negative charges and, at pH 5, the missing negative charges lead to a more flexible, displaced pattern of bound calcium ions. Only one of two carboxyl groups per side chain of γ-carboxylglutamate (U) is then deprotonated, the Gla domain thus bears a positive charge (Figure 1b and Figure 5a). The calcium ions are more flexibly bound, redistribute, and osteocalcin gains conformation flexibility (Figure 5a). Residues U17 and U21 no longer bind the calcium ions, of which one migrates to D30 and to D34 that fully compensate the local electrical charge. The other calcium ion migrates to U24, which now coordinates two calcium ions, consistent with a stabilizing effect of positively charged ions near the carboxyl end of an α-helix (Figure 5a). The effective charge of the U24 residue is now up to +3e and attracts negatively charged H₂PO₄ ions, supporting adsorption and prenucleation of dihydrogen phosphate ions at the modified Gla site at pH 5 (Figure 5b, c). The native protein structure at pH 7, in contrast, has no affinity to adsorb protonated phosphate anions since all six carboxyl groups U17, U21, and U44 in the Gla domain carry negative charges and coordinate 3 calcium ions, equal to an effective charge of zero (Figure 5a, d).

S2. Additional Details of Calcium Phosphate Nucleation

In addition to the more common (010) and (001) surfaces, we observed a similar mechanism of calcium phosphate nucleation on the tricalcium motif of osteocalcin on the less common HAp (101) surface. The (101) surface shows a higher concentration of 35 ± 1 mM of desorbed phosphate ions than the (001) surface with a corresponding value of 22.7 ± 0.5 mM at pH 5 and shows a similarly sharp decrease in surface dissolution of calcium phosphate species at pH 7.

S3. Summary of Key Findings

Osteocalcin is a non-collagenous protein in bone and found to adsorb onto the major

crystallographic surfaces of HAp, especially under slightly acidic conditions at pH ~5 and somewhat weaker at pH ~7. The tri-calcium domain including three calcium ions avoids interactions with all HAp (hkl) surfaces, and the motif can act as a nucleation site for the growth of HAp at pH ~5 when it carries an effective positive charge. Dihydrogen phosphate and calcium ions readily adsorb onto the motif and are stabilized on the protein surface upon an increase in pH to ~7 as osteoblasts release phosphate ions. Then, growing prenucleation clusters containing monohydrogen phosphate remain attracted to these sites, enabling nucleation and growth of new HAp. In this manner, osteocalcin initiates the bone remodeling process at the molecular scale. At a neutral pH of ~7 or higher, the Gla site on native osteocalcin is effectively charge-neutral and has marginal interactions with phosphate species and calcium ions in solution. Soluble hydrogen phosphate and calcium ions prefer to form pre-nucleation clusters in solution rather than adsorption onto the native protein surface. Osteocalcin inhibits further growth of nearby HAp crystallites via binding to the HAp (010) and (101) surfaces. The mechanistic proposal and simulation techniques allow further tests and modifications of the process from the molecular scale.

In summary, molecular dynamics simulations in comparison with extensive experimental data suggest that the initial bone remodeling process by osteocalcin involves protein adsorption on the HAp surface at pH 5, nucleation of dihydrogen phosphate on the tri-calcium motif, and conversion into monohydrogen phosphate and further growth of calcium phosphate nuclei as the pH value increases to 7. At pH 7 in the native state, osteocalcin and the Gla domain have no preference to nucleate calcium phosphate from scratch, and prenucleation is preferred in solution. We explained differences in the structure of osteocalcin at pH 5 compared to its native structure at pH 7 (Figure 5a) and illustrate dynamic changes in the protonation and adsorption of phosphate species, as well as in the adsorption of calcium ions, that affect protein-mediated nucleation and growth of new

HAp. Experimental studies will be needed to further evaluate and develop the proposed mechanism as advances in instrumentation will allow insight at the molecular scale.

Supporting Reference

(1) Nelson, D. L.; Cox, M. M., *Lehninger Principles of Biochemistry*. 5th ed.; W.H. Freeman and Company: New York, USA, 2008.